Non-peer-reviewed preprint submitted to EarthArXiv

Seasonal-reference and regularization sensitivity with weak annual chlorophyll prediction

Luigi Caputi

ORCID: https://orcid.org/0000-0002-5724-1943

Università Telematica San Raffaele, Via di Val Cannuta 247, 00166 Rome, Italy

Correspondence: luigi.caputi@uniroma5.it

Peer-review status. This manuscript is a preprint submitted to EarthArXiv and has **not been peer reviewed**. It has not been accepted for publication in any journal. Later versions may differ in content. If a peer-reviewed version is published, it will be linked from this preprint's EarthArXiv page through the "Peer-reviewed Publication DOI" field.

Keywords: marine heatwaves; ocean colour; surface chlorophyll; phytoplankton seasonality; ridge regression; model selection; cross-validation; preprocessing leakage

Preprint version: 11 November 2026

Seasonal-reference and regularization sensitivity with weak annual chlorophyll prediction

Luigi Caputi[1,*]
[1]Università Telematica San Raffaele, Via di Val Cannuta 247, 00166 Rome, Italy
[*]Correspondence: luigi.caputi@uniroma5.it

11 November 2026

Abstract

Do bloom-phase heatwave exposures improve annual surface-chlorophyll anomaly prediction beyond a nutrient-aware baseline? We compare two historical seasonal-reference constructions on fixed later-year evaluation cases, outcomes and inputs. The best pooled error on the original model and penalty grid is less than 4% below zero-anomaly prediction, which predicts the calibrated seasonal-reference integral; primary conditional bands for benchmark gains include zero, with coverage unvalidated. Under fixed historical geometry, an apparent selected-procedure advantage depends on nearly tied coarse-grid tuning, while full and baseline model errors are nearly identical at penalty 1000. A retrospective one-standard-error rule selects 1000 for every pooled model under both constructions and removes the large reversal; it is not a validated remedy. Competing troughs exchange rank and move annual boundaries. Joint response and predictor substitution for ten extreme historical windows is conditionally sufficient to reproduce the penalty switch; substituting their whole complement is not. Cross-scoring shows prediction changes and target changes each reverse the tested penalty pair. With original targets fixed, both errors increase; the weaker penalty deteriorates more. Target substitution alone yields a near-zero reversal. Both constructions share a dense-grid minimum and broad near-optimal region. Report calibrated benchmarks and paired selection losses, and justify the scientific target before freezing preprocessing and selection for independent evaluation.

1 Introduction

Marine heatwaves can affect phytoplankton differently across seasons and nutrient environments (Hayashida, Matear, and Strutton 2020; Noh, Lim, and Kug 2022; Wyatt, Resplandy, and Marchetti 2022). We ask whether bloom-phase exposure and its additional interactions with climatological nitrate improve annual surface-chlorophyll prediction beyond severity, calendar, nutrient, geography and trend predictors. Chlorophyll motivates this prediction task but does not directly measure primary production or physiological limitation.

The distinctive issue is the interaction of two discrete decisions. A seasonal trough defines annual integration windows and allocates heatwave exposure among phases; nearly tied development losses then select a ridge penalty. Changing the reference can therefore change both constructed observations and the selected procedure. A large fitted-model comparison followed such a change, although the recorded ecological criterion—at least 10% improvement over the baseline, with uncertainty and additional comparator requirements—failed (Supplement S11). We examine whether that apparent gain adds skill beyond the calibrated reference for annual anomalies and how the two decisions connect.

Selection bias concerns optimizing a noisy criterion (Varma and Simon 2006; Cawley and Talbot 2010); instability concerns changes in the chosen procedure (Breiman 1996). Preprocessing before fold separation creates a distinct dependence problem (Moscovich and Rosset 2022), while structured validation must match the prediction setting (Roberts et al. 2017; Furtado et al. 2026). Here,

constant benchmarks establish the skill context, reconstructed seasonal curves expose competing troughs, and a fixed-identity intervention tests their connection to tuning. Retained predictions then separate prediction changes from changes in the scoring targets. These retrospective diagnostics explain this pipeline; they do not select a replacement model from evaluation outcomes.

2 Data and methods

2.1 Observations and annual response

The intended panel contains 48 one-degree tiles at 25, 35, 45 and 55°N, with six longitudes per basin: 50, 44, 38, 32, 26 and 20°W in the Atlantic, and 170, 164, 158, 152, 146 and 140°W in the Pacific. Of 1296 candidate tile-year windows, 693 pass annual support and 666 also pass seasonal support. No window at 55°N qualifies, so the realized comparison spans 25–45°N. The latitude-specific seasonal counts are 280, 296, 90 and zero; Table S16 shows basin, period and split attrition.

Daily sea-surface temperature is NOAA OISST version 2.1 for 1982–2024 (B. Huang et al. 2020; Boyin Huang et al. 2021). Chlorophyll is ESA OC-CCI version 6.0 for 1998–2024 (European Space Agency 2023; Sathyendranath et al. 2019). Its provisional 2023–2024 extension was accessed on 7 October 2026 through the version-6 aggregation and lies beyond the cited archive ending in 2022. Native cells are area-averaged within tiles; chlorophyll composites retain their actual durations. Usable composites observe at least 20% of an empirical water mask, defined by the union of observed pixels over all downloaded 1998–2024 years. This denominator can therefore let later availability affect earlier coverage eligibility, without inserting later chlorophyll magnitudes into earlier tile means. Nitrate is the equal-month December–February surface climatology from World Ocean Atlas 2023 (Garcia et al. 2024), transformed as $n = \log[1 + N/(1\,\mu\mathrm{mol\,kg^{-1}})]$.

A positive seasonal reference $C_0(t)$ is fitted to 1998–2013 log chlorophyll using three Fourier harmonics, duration weights and residual-smearing correction. A biological year begins at the reference minimum. Its annual anomaly is

$$B_W = \int_W C_0(t)\,dt, \qquad Q_W = \frac{\int_W C(t)\,dt}{B_W} - 1.$$

Thus zero predicts an annual integral equal to its reference, and an absolute error of 0.11 represents 11% of the reference integral. Eligible windows require at least 80% observed intervals and days, no gap longer than 24 days, complete boundaries and at least ten coverage-qualified reference years. Other partially observed years may contribute to fitting. Short bounded gaps interpolate the observed/reference ratio. Phase eligibility requires a peak-to-trough ratio of at least 1.5 and a dominant peak at least 1.25 times a secondary peak separated by 60 days.

2.2 Reference constructions and prediction models

With **window-specific geometry**, each historical target excludes both calendar years it touches from reference fitting; that fit supplies its concentration curve, annual boundaries and phase landmarks. With **fixed historical geometry**, the target-excluded concentration curve is retained, while boundaries and landmarks use all available 1998–2013 observations. Evaluation uses the full historical reference in both constructions. Historical outcomes and exposures change; evaluation outcomes, inputs and cases remain fixed. Numerical files label the constructions `original` and `both`. Target-year exclusion is not fold-wide exclusion: other validation-fold years remain in the concentration fit, and fixed historical landmarks also use the target years. Internal validation is conditional on shared, response-derived preprocessing. Shared historical calibration alone does not establish use of later chlorophyll outcomes in reference fitting. Table S18 distinguishes these dependencies from fold-isolated scaling, later-period coverage access, climatological descriptors and reconstruction at window edges.

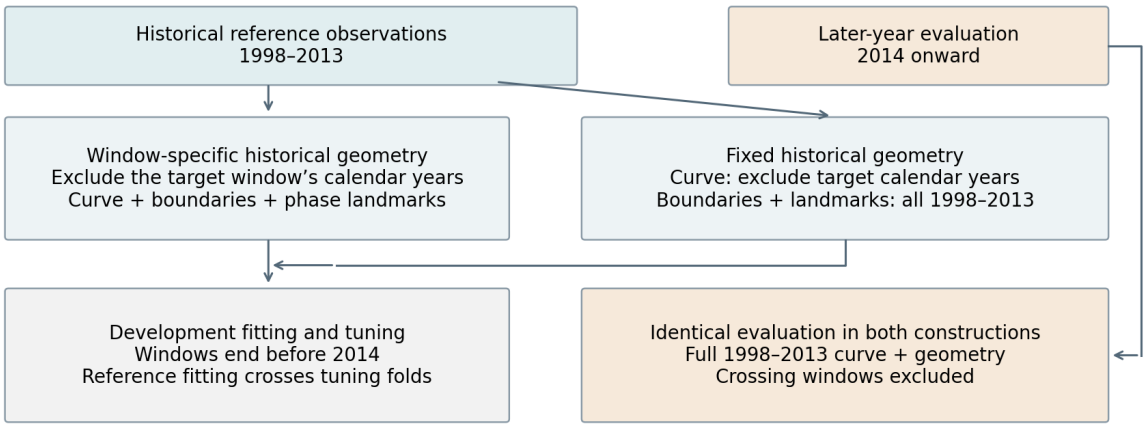


Figure 1. Reference calibration and evaluation. Historical geometry changes while the concentration curve remains target-excluded. Evaluation geometry and outcomes are identical across constructions. References share historical observations across subsequent tuning folds.

Marine heatwaves follow the Hobday definition (Hobday et al. 2016) and specified reference implementation (Oliver, n.d.), using the local 90th percentile over 1982–2011, an 11-day calendar window, 31-day smoothing, at least five exceedance days and joining across gaps of at most two days. Positive excess-temperature dose above the seasonal mean is assigned to pre-bloom, rising, declining and remaining phases using reference landmarks. Calendar controls are signed sine and cosine dose sums. Exact landmark, phase, leap-day and zero-exposure definitions are in Supplement S10.

All eligible years, including those without heatwaves, enter the analysis. Exposures cover the outcome window, making this retrospective conditional prediction rather than advance forecasting. The baseline M0 already contains nitrate interactions with severity and calendar terms. The phase increment is therefore specific, not a test of whether nutrient information helps at all.

Table 1. Predictor sets. Counts exclude the intercept.

Model	Columns	Predictors
M0	16	Severity, nitrate and their interactions; geography; trend; first calendar harmonic and its nitrate interactions
Mphase	19	M0 plus three phase doses, omitting remaining-phase dose
M1	22	Mphase plus three phase-dose × nitrate interactions
Mcalendar	24	M0 plus second and third calendar harmonics and their nitrate interactions

Ridge regression minimizes $\sum_i (y_i - b - \mathbf{z}_i^T \boldsymbol{\beta})^2 + \alpha \|\boldsymbol{\beta}\|^2$, with training-only centering/scaling and an unpenalized intercept. Geography uses latitude and basin-relative longitude and their squares, centered at 35°W and 155°W, and all models include a linear year term. The original penalty grid is $\{0.1, 1, 10, 100, 1000\}$. Effective degrees of freedom (EDF) are $1 + \sum_j d_j^2/(d_j^2 + \alpha)$ for standardized training-design singular values d_j. Equal penalties need not give equal EDF (Hastie 2020). Because the objective sums squared errors, its per-observation penalty is α/n; comparing penalty numbers across training sizes requires that scale distinction. The weight-normalized chronology sensitivity addresses this issue (Supplement S9).

2.3 Development evaluation and controlled comparisons

Development windows end before 2014; evaluation windows start in 2014 or later, with crossing windows excluded. Pooled evaluation trains on both basins; the two transfer scenarios train on one basin and evaluate the other. Evaluation requires source-training-range inclusion for nitrate, latitude, severity and relative longitude. This fixed, outcome-independent screen gives training/evaluation sizes of 367/211, 222/77 and 145/76. It does not guarantee joint covariate overlap. Evaluation biological-year labels are 2014–2023, with some windows containing 2024 days.

Development selection minimizes pooled-row mean absolute error (MAE) across grouped four-year folds, with adjacent years purged. Training can occur before and after a held-out block. Fitting requires at least 20 training observations, five validation observations and two usable folds; exact ties favor the larger penalty. A retrospective one-standard-error rule chooses the largest penalty whose loss is within a heuristic fold SE of the minimum. Shared calibration, dependent cases and overlapping training sets prevent interpreting that SE as calibrated uncertainty (Bengio and Grandvalet 2004; Varoquaux 2018). Its formula is retained in Supplement S11.

We evaluate all models and original penalties on the same cases, alongside zero, source-training-mean and source-training-median predictors. Relative gain is $1 - \mathrm{MAE}_{first}/\mathrm{MAE}_{comparator}$; a negative paired MAE difference favors the first fit. The comparison targets differ (Table 2); none alone isolates an ecological effect of phase-specific exposure.

Table 2. Interpretation of model comparisons.

Comparison	Target of the comparison	Attribution limit
Independently selected penalties	Whole procedures, including their tuning decisions	Model design and regularization both differ
Common penalty	Fitted specifications at a particular penalty	Total flexibility can still differ
Equal EDF	Specifications at a particular total smoother trace	Directional shrinkage and predictor representation still differ

Further development-only diagnostics retain 63 penalties and alternative historical chronologies. Reference diagnostics reconstruct all large boundary shifts. A four-state intervention retains the same 367 historical identities and four folds, jointly replacing Q and every model predictor for none, only the ten previously identified extreme windows, only the other 357, or all windows. The mask is defined by at least 90 days of actual boundary displacement, not loss influence. Training scaling and fitting are recomputed for each state; substituted validation targets also change. We report full development curves and $\Delta_{\mathrm{CV}} = \mathrm{MAE}_{\mathrm{CV}}(1000) - \mathrm{MAE}_{\mathrm{CV}}(100)$, preserving nonadditivity across subsets. These are computational interventions on constructed observations, not alternative ecological datasets or prospective validation.

We then cross-score the retained predictions at 100 and 1000 against original and substituted Q on identical keyed rows. For prediction source p and target source s (0 original, 1 substituted), define $D_{ps} = n^{-1} \sum_i (|\hat{Q}^{(p)}_{i,1000} - Q^{(s)}_i| - |\hat{Q}^{(p)}_{i,100} - Q^{(s)}_i|)$. We retain both change orders and the interaction $D_{11} - D_{10} - D_{01} + D_{00}$. No additional fit or evaluation score is needed.

A separate support audit counts overlaps, gaps and unique usable-composite tile-days without changing eligibility or scoring new evaluation models. Conditional uncertainty uses paired two-way spatial/temporal resampling of fixed predictions, with four temporal evaluation groups. Bands are nominal and their coverage is unvalidated. They are not adjusted for multiple exploratory comparisons. Supplement S11 gives full procedures; Supplements S1–S9 retain every comparison, sensitivity and original ecological result.

3 Results

3.1 Limited gains beyond the calibrated reference

The best pooled point errors among the original model designs and penalty grid are only slightly below zero-anomaly prediction: the annual integral of the calibrated seasonal reference. At penalty 1000, window-specific M1 has 3.62% lower MAE than zero; Mphase has the lowest original-grid pooled error, improving by 3.80%, or 3.96% under fixed historical geometry. These are evaluated point comparisons, not replacement model selections. Models selected at penalty 100 perform worse than those benchmarks (Table 3). For the window-specific pooled contrast at 1000, M1 minus M0 is +0.000031 with a conditional nominal 95% band [−0.00415, +0.00327] (Table S13); near-identical point error is not evidence of equivalence. As supporting detail, all 72 primary null-relative bands span zero. They reuse outcomes, models and benchmarks and are not independent confirmations of a null result; their coverage is unvalidated.

Table 3. Absolute benchmarks under window-specific geometry. The final two columns use penalty 1000.

Scenario	Zero	Train mean	Train median	M0	M1
Pooled	0.116358	0.117078	0.115308	0.112112	0.112143
Atlantic to Pacific	0.109224	0.111263	0.105987	0.101291	0.095475
Pacific to Atlantic	0.104382	0.104367	0.104872	0.106569	0.106311

The retrospective **one-standard-error rule selects penalty 1000 for every pooled model under both constructions** (Table S4). The large apparent reversal consequently disappears under that rule. Exact-minimum selection instead chooses M1 at 100 with window-specific geometry and 1000 with fixed historical geometry. Under the latter construction, the development-loss difference between these penalties is only 0.000163, compared with a heuristic fold SE of 0.009495. Paired fold differences show the cancellation directly (Table 4). The SE of absolute fold losses is not an SE for the paired difference, and four dependent folds are insufficient for calibrated inference. The one-standard-error result establishes sensitivity to another selection policy; it identifies neither an optimal penalty nor a validated remedy.

Table 4. Paired M1 development-loss differences, MAE(1000) minus MAE(100). Negative favors 1000. These four dependent folds do not support calibrated inference; the SE of absolute fold losses is not the SE of these paired differences.

Validation labels	Cases	Window-specific	Fixed historical
1998–2001	82	0.0075109	0.0073246
2002–2005	103	-0.0002934	-0.0006785
2006–2009	103	-0.0078586	-0.0084826
2010–2012	79	0.0036330	0.0035834

The previously emphasized 15.08% M1–M0 advantage under independently selected fixed-historical models is therefore a coarse-grid result sensitive to a near tie. It describes the realized procedures but provides weak support for an ecological predictor increment. The denser grid and matched controls below clarify that sensitivity. The original recorded ecological criterion is unmet, and none of the original-grid Pacific-to-Atlantic models beats zero or the training-mean benchmark.

3.2 Matched controls limit predictor attribution

At penalty 1000, M0 and M1 have nearly identical pooled MAEs under either construction (Table 5). In pooled evaluation, window-specific M1 is worse than M0 at every original-grid penalty; Mphase is better than M1 at every original-grid penalty under both constructions. Most of the original headline improvement is reproduced by stronger baseline regularization. The exact arithmetic and alternative controls are retained in Supplement S11.

Table 5. Pooled comparisons on 211 fixed cases. Asterisks mark the exact minimum-development-loss fit for each model and construction. EDF includes the intercept and is calculated on the full training design. A common penalty does not equalize EDF.

Geometry	Penalty	M0 MAE	M0 EDF	M1 MAE	M1 EDF	M1 minus M0
Window-specific	100	0.132673*	9.956	0.135845*	12.480	0.003171
Window-specific	1000	0.112112	4.276	0.112143	5.249	0.000031
Fixed historical	100	0.131828*	9.952	0.134754	12.468	0.002926
Fixed historical	1000	0.111963	4.276	0.111952*	5.250	-0.000011

Common penalties leave models with different flexibility. Under window-specific geometry, equal-EDF comparisons retain some M1–M0 point improvements, but at EDF 8, 10 and 14 M1 is worse than zero; all four models are worse at EDF 10 and 14. Mcalendar remains better than zero at EDF 8, and Mphase is better at EDF 6. These distinctions constrain claims about skill beyond the calibrated reference for annual anomalies (Table S12). Direction-dependent transfer and phase-encoding results likewise qualify a universal absence of predictive information, while leaving the ecological criterion unsupported.

3.3 Trough choice and near-tied penalties define two discrete decisions

Across 367 historical windows, the median absolute start-date change is two days. Yet ten windows in five tiles move by at least 90 days and account for 64.56% of total absolute response change. Exact refits show exchanges in the ranking of competing seasonal troughs (Figure 3). Their local-minimum locations move by at most five phase days, while curve changes are small relative to seasonal amplitude. Selecting a different trough, rather than moving the same trough by months, creates the large anchor shifts. Dominant-peak eligibility does not ensure a stable minimum-based annual boundary.

The maximum 225-day shift is between actual start dates in the same labeled year: 22 January and 3 September 2004 at Atlantic 45°N, 20°W. The corresponding shortest circular displacement is −141 phase days. It is a change in annual-window construction, not a measured displacement of the ecological season. This geometric result alone does not identify tuning influence; the intervention below tests that connection.

On the denser development grid, **both constructions select the same best tested M1 penalty, 398.11**, and the same M0 penalty, 112.20 (Figure 4). The conspicuous 100-to-1000 switch reflects loss ordering on a coarse candidate grid, rather than evidence for a tenfold change in preferred regularization. The sampled M1 penalties within 1% of minimum development MAE span 112.20–891.25 under both complete constructions, almost an eightfold range. M0 spans 14.13–281.84 and 17.78–316.23, respectively. These descriptive tolerance ranges show a broad trough; they are not

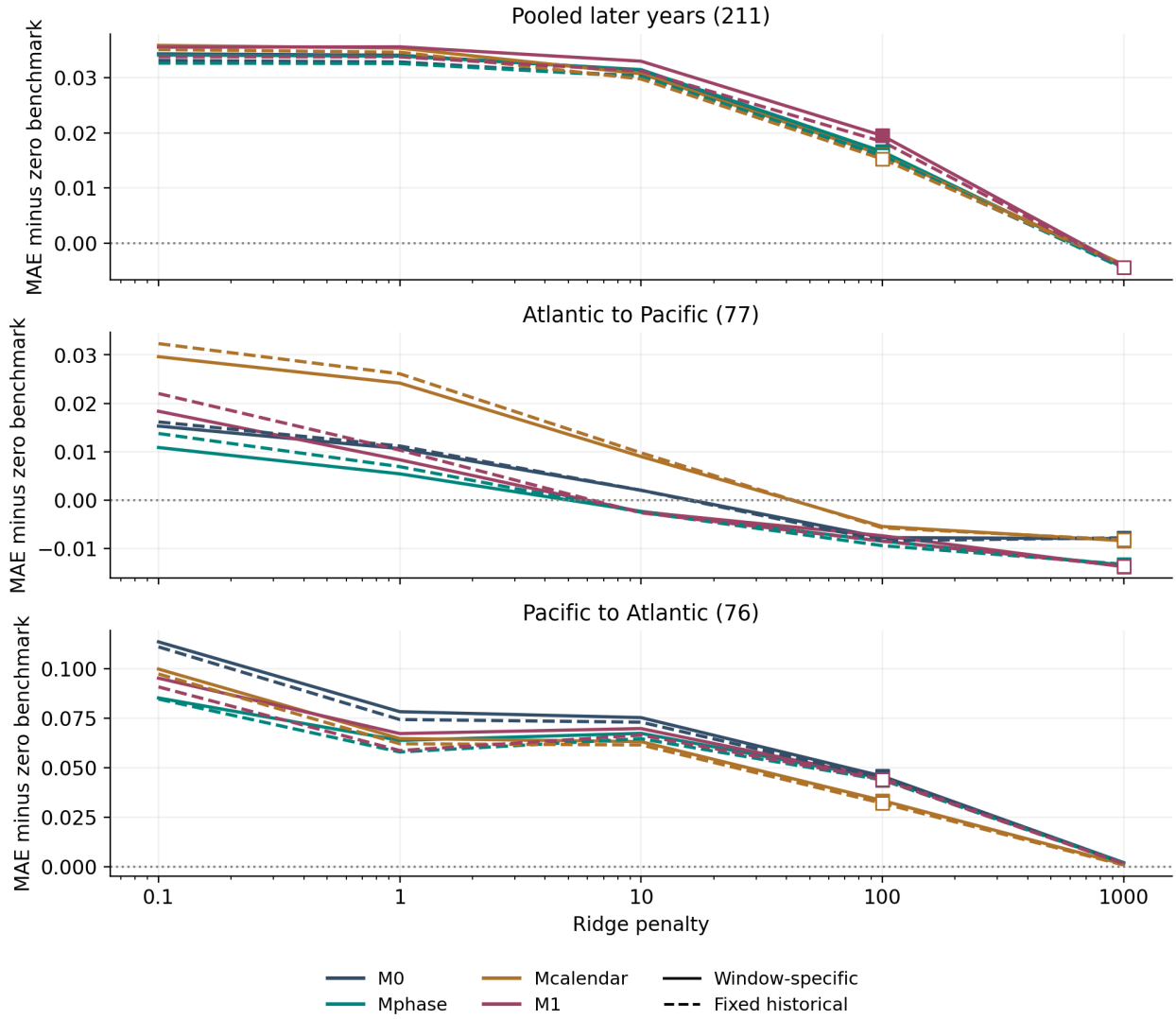


Figure 2. Original-grid evaluation MAE minus the zero-anomaly benchmark on fixed cases; negative values favor the fitted model. Squares mark exact-minimum development selection, filled for window-specific and open for fixed historical geometry. Curves can overlap. Vertical scales differ across scenarios. Tables S1a–S1f retain absolute evaluation and development MAEs.

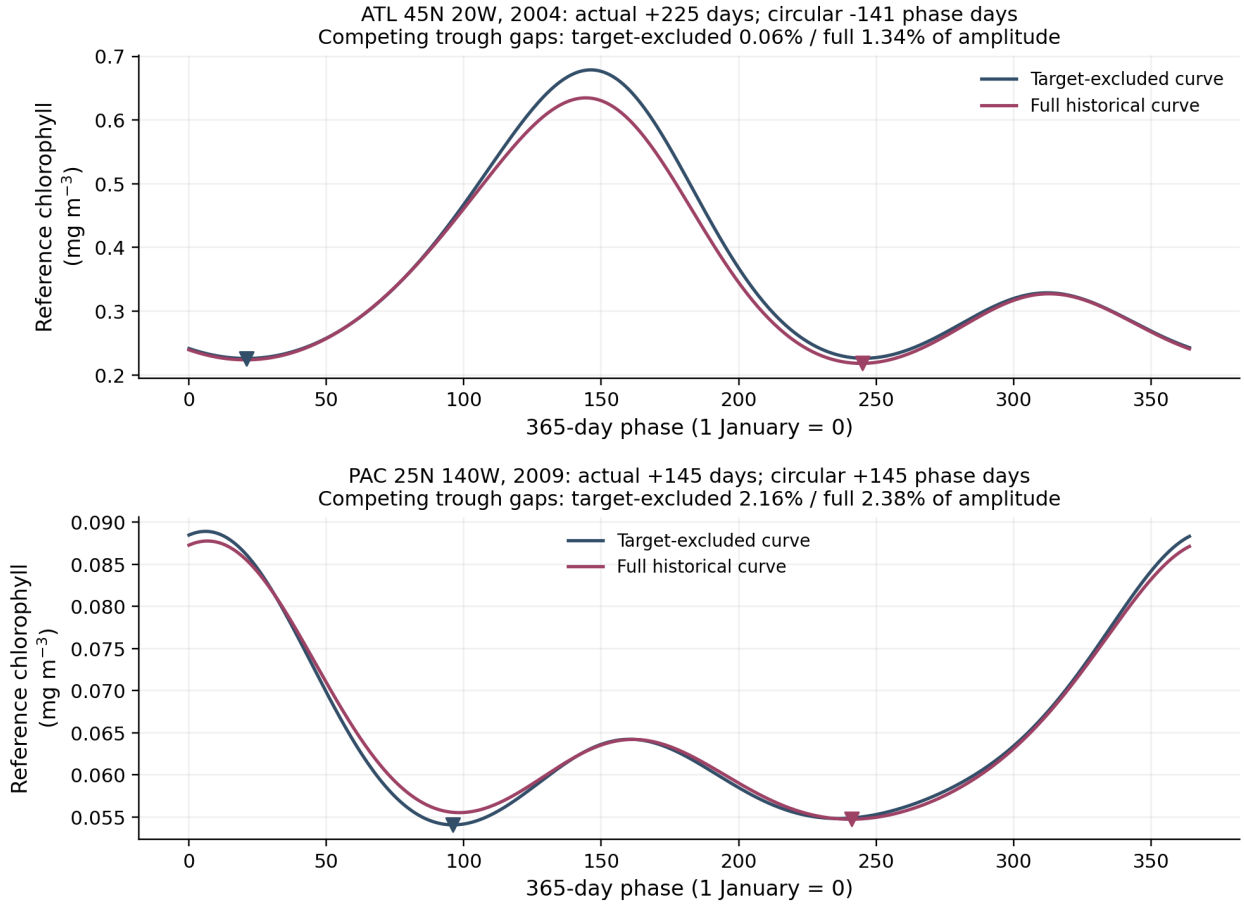


Figure 3. Competing troughs and annual-boundary selection. The largest actual-date displacement is shown above and the largest shortest-circular displacement below. Triangles mark the selected minima of target-excluded and full historical curves. Fixed historical geometry uses the full curve's landmarks while retaining the target-excluded concentration curve. The annotated competing-trough gaps are depth differences from each curve's global minimum, normalized by that curve's seasonal amplitude. Small depth changes exchange the preferred annual anchor. Tables S10–S11 retain the distribution and all ten extreme cases.

confidence regions or recommended penalties. Later-year performance under dense-grid selection was not evaluated.

3.4 The extreme-window intervention reproduces the coarse switch

Changing only the ten extreme windows reverses the M1 margin from +0.0001723 to −0.0002701 and selects 1000 on the original grid. Changing only the remaining 357 leaves a positive margin, +0.0002103, and selects 100. Changing all windows gives −0.0001632 and selects 1000 (Table 6; Figure 4). Thus the joint changes in those ten constructed rows are sufficient to reproduce the switch in this fixed experiment; restoring them to original values while changing the complement removes it. All four states still contain folds favoring each penalty. This establishes conditional sufficiency of the joint ten-row substitution, not that every row is necessary or that the set is minimal or unique. A differently chosen subset of the other 357 could still reverse the near tie, despite cancellation in their aggregate.

Table 6. Joint historical response/predictor substitutions on the same 367 identities and four folds. Margins are development MAE(1000) minus MAE(100). M0 retains coarse penalty 100 and dense penalty 112.20 throughout. No later-year score is computed.

Changed rows	Count	M0 margin	M1 margin	M1 coarse alpha	M1 dense alpha
None	0	0.0047146	0.0001723	100	398.11
Extreme ten	10	0.0042050	-0.0002701	1000	446.68
Other 357	357	0.0046227	0.0002103	100	398.11
All 367	367	0.0041379	-0.0001632	1000	398.11

The total margin change, −0.0003355, equals the extreme-subset change −0.0004424, the complement change +0.0000380, and their nonadditivity +0.0000689. This accounting does not assign a unique causal percentage. Q, predictors, scaling and refitted predictions change together, including substituted validation outcomes; displaced dates alone are not isolated. M0 selects coarse penalty 100 throughout. Dense M1 minima remain 398.11 except for the extreme-only state, 446.68. No later-year model is selected or evaluated by this experiment.

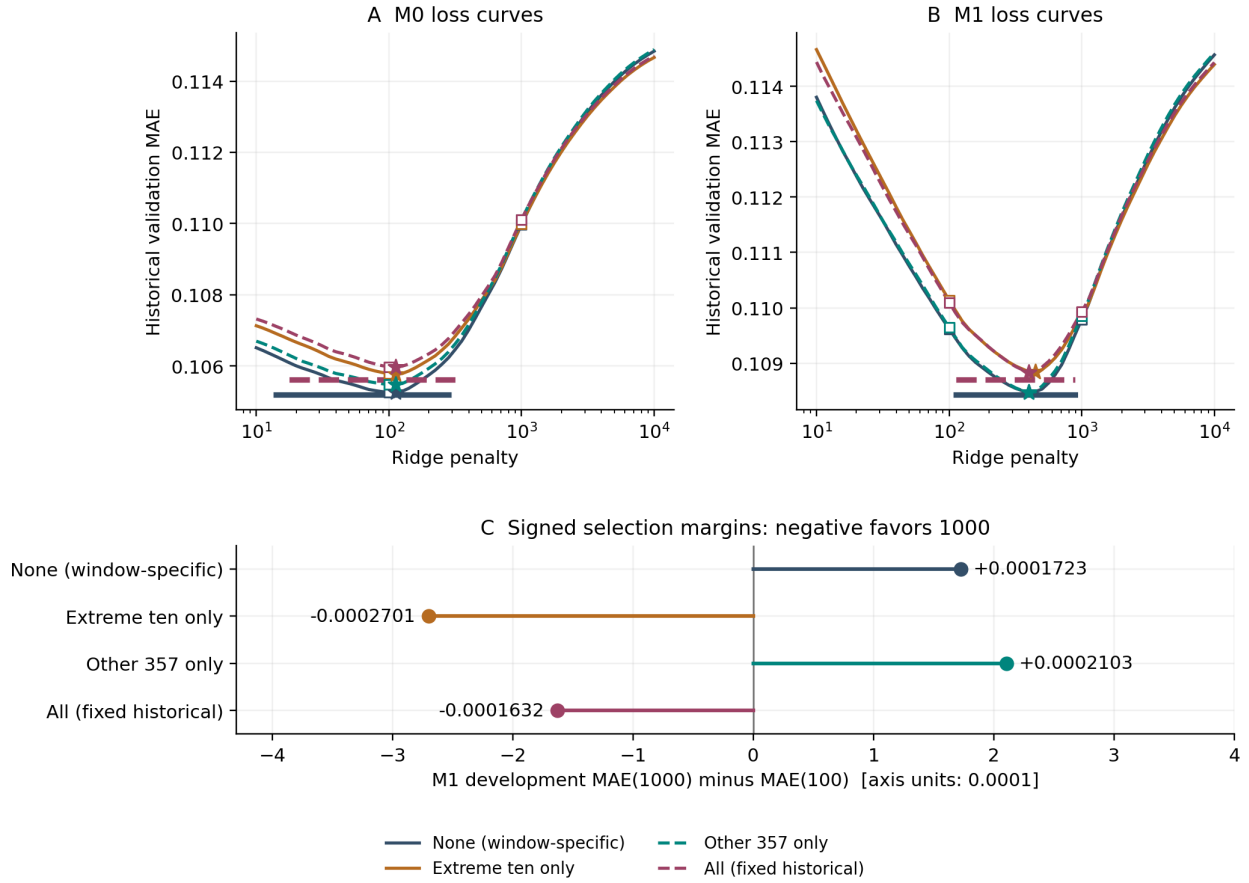


Figure 4. Two model loss curves and four signed M1 selection margins for joint historical row substitutions. Curves retain 63 penalties; panels A–B display 10–10000, squares mark 100 and 1000, and stars mark sampled minima. Vertical scales differ. Short solid and dashed segments show the window-specific and fixed-historical sampled ranges within 1% of minimum MAE. Panel C enlarges the decisive margins around zero; negative favors 1000 over 100. All conditions retain 367 identities and four folds.

3.4.1 Cross-scoring separates prediction and target changes

In the extreme-ten cross-score, changing predictions while keeping original Q gives a margin of −0.0000790; changing Q while keeping original predictions gives −0.0000111 (Table 7). Thus either route alone reverses the 1000-versus-100 ordering. These mixed-construction scores do not establish full-grid choices or identify either Q definition as ecological ground truth. M0's four corresponding margins remain positive.

Table 7. M1 cross-scored development margins, MAE(1000) minus MAE(100), on the same 367 historical identities, using saved predictions at each penalty. Negative favors 1000 over 100. Off-diagonal cells mix prediction and target constructions; they are algebraic diagnostics, not new fitted procedures or full-grid selections.

Prediction source	Original outcomes	Extreme-ten outcomes
Original	+0.0001723	-0.0000111
Extreme ten	-0.0000790	-0.0002701

With original Q held fixed, both penalties' MAEs increase (100: 0.109619 to 0.109976; 1000: 0.109791 to 0.109897). The ranking reverses because 100 deteriorates more. Target substitution alone crosses this particular selection boundary by only −0.0000111; it does not establish a substantively preferable penalty. This sensitivity near a tie is consistent with the broad development-loss trough.

The total M1 margin change is −0.0004424. Changing predictions first contributes −0.0002513, followed by −0.0001911 from targets. Reversing the order gives −0.0001835 from targets and then −0.0002589 from predictions; the interaction is −0.0000076. The prediction contribution is somewhat larger in both orders, but target redefinition is material. The prediction route combines changed fitting, scaling and validation predictors. Both losses, fold accounting and secondary cross-scores remain in the numerical results.

3.5 Annual construction changes observation support

Window-specific annual boundaries need not partition time. Across 329 consecutive-label historical pairs, they create 841 overlapping and 1143 intervening calendar tile-days; fixed historical boundaries create neither. Thirteen pairs touching the extreme windows account for 478 overlap and 707 gap tile-days. On the same 367 rows, unique usable-composite support is 127486 versus 128276 tile-days (Table S15). Row-weighted MAE assigns equal weight to constructed annual observations, not to unique days or independent satellite acquisitions.

The eight construction-by-fold checks find no shared nominal days, usable days, interpolation-bracket support or composite identities between purged training and validation rows. This supports the implemented purge, not independence of their shared reference fits. The 274 later seasonal windows before marginal-support screening have identical support under both constructions. Coverage distributions and inherited stricter-support results appear in Supplement S12. Raising pixel coverage to 30% retains 634 of 666 seasonal windows and changes some Q values; temporal interpolation and these filters do not establish harmless variation in the native satellite footprint.

3.6 Temporal concentration and residual prediction errors

Stronger shrinkage attenuates a poorly extrapolating negative trend, but its pooled benefit is concentrated in a short later interval. Biological-year labels 2020–2022 contain 59 of 211 evaluation cases and account for 66.41% of M0's and 67.75% of M1's total absolute-error reduction from penalty 100 to 1000. Label 2023 contributes about another 15%. This concentration, within only four temporal groups, limits generalization across time; it is not an independently established ecological regime shift.

Substantial basin offsets persist after shrinkage. At penalty 1000, window-specific M1 mean prediction-minus-observation bias is −0.057 in the Atlantic and +0.029 in the Pacific; M0 biases are −0.053 and +0.034. Supplement S11 and Figure S2 give trend, year and basin diagnostics. A quadratic-trend variant is particularly unstable in Pacific-to-Atlantic transfer, with M1/M0 MAEs of approximately 0.499/0.507 (Table S6c). These residual errors reinforce the limited gains beyond the anomaly benchmarks.

4 Discussion

This case connects two discrete decisions: the seasonal trough defining constructed observations and the penalty selected from nearly tied development losses. The ten-window substitution reproduces the switch; its complement does not. Yet the tested models add little pooled, original-grid skill beyond the calibrated seasonal-reference benchmark. Zero Q already predicts the fitted reference integral, so this finding does not establish that raw annual chlorophyll is nearly unpredictable. Equal-EDF and transfer results preserve smaller, procedure-dependent possibilities.

Cross-scoring exposes both prediction and target sensitivity. With original outcomes fixed, both penalties perform worse after substitution; 100 deteriorates more. Target changes alone also cross the near-tied boundary, by only −0.0000111. These results establish conditional sufficiency, without identifying indispensable observations, a pure training-data effect or a substantively superior penalty.

A strong seasonal peak can coexist with competing shallow minima. Reference stability therefore matters even when peak eligibility is unchanged. This connects selection instability (Breiman 1996), preprocessing dependence (Moscovich and Rosset 2022) and leakage in prediction studies (Kapoor and Narayanan 2023; Furtado et al. 2026). Report reference benchmarks and paired development losses alongside selected procedures. Freeze preprocessing, selection and meaningful-improvement criteria before independent evaluation; the recorded 10% criterion has unverified prospective provenance. Retaining alternative analytical choices makes their consequences inspectable (Steegen et al. 2016; Simonsohn, Simmons, and Nelson 2020).

Three limitations govern interpretation. Reference fitting crosses tuning folds, and all-year satellite masks affect historical eligibility (Table S18), although shared calibration alone does not demonstrate contamination by later chlorophyll magnitudes. Separate calibration needs longer coverage-qualified histories and more separated development blocks; its support thresholds remain unchanged. Uncertainty is conditional, supported by only four primary temporal groups, and not validated by the mismatched simulation; general time-series results do not remove those limitations (Bergmeir, Hyndman, and Koo 2018). Finally, the realized population excludes 55°N, and annual surface chlorophyll with climatological nitrate cannot identify physiological mechanisms. Weak benchmark-relative gains do not establish ecological absence.

Stabilizing selection and defining a scientifically meaningful annual target remain separate tasks. Numerical stability cannot establish whether seasonal-minimum years, calendar windows or independently calibrated boundaries best represent the ecological quantity. That choice requires scientific justification before model selection; the present diagnostic does not resolve it.

5 Data availability and research assistance

The source products are NOAA OISST v2.1, ESA OC-CCI v6 and World Ocean Atlas 2023, identified by the cited data records and the accompanying data manifest. The 2023–2024 chlorophyll extension came from the live v6 service and is not covered by the cited archive ending in 2022. Study-specific derived inputs and retained predictions are not publicly archived. The original analysis software is open source under GPL-3.0-or-later, with third-party attribution preserved.

AI systems assisted UCP Technology LLC with computation, code, literature review and writing. AI numerical and adversarial checks do not constitute independent human scientific validation.

Supplementary scientific material

Supplement navigation	Evidence and role
Primary comparisons and construction diagnostics	S1–S3, S9 and S11; complete grids, fold losses, reference refits and attribution
Diagnostic sensitivities and implementation	S4–S5, S10 and S12; variants, influence, exposure definitions and observation support
Historical ecological analyses	S8; retained hypotheses and annual accounting
Failed or limited validation attempts	S6 separate calibration; S7 mismatched coverage stress test

S1 Complete original penalty grid

All scores use the original fixed evaluation outcomes and model inputs. The changed construction alters historical responses and design only. Response-only and predictor-only substitutions are reported in Table S5. Asterisks denote exact development selection within a model, not the best evaluation score. Each cell below is evaluation MAE / development MAE.

Table S1a. Pooled, window-specific construction.

Penalty	M0	Mphase	Mcalendar	M1
0.1	0.15067 / 0.10889	0.15045 / 0.11296	0.15220 / 0.11577	0.15186 / 0.12024
1	0.15041 / 0.10740	0.15026 / 0.11130	0.15170 / 0.11542	0.15194 / 0.11825
10	0.14770 / 0.10651	0.14780 / 0.10985	0.14706 / 0.11405	0.14933 / 0.11380
100	0.13267 / 0.10526*	0.13297 / 0.10764*	0.13235 / 0.10793*	0.13584 / 0.10962*
1000	0.11211 / 0.10997	0.11193 / 0.10921	0.11248 / 0.11032	0.11214 / 0.10979

Table S1b. Pooled, fixed historical construction.

Penalty	M0	Mphase	Mcalendar	M1
0.1	0.14946 / 0.10903	0.14898 / 0.11282	0.15143 / 0.11581	0.15013 / 0.11910
1	0.14920 / 0.10773	0.14891 / 0.11136	0.15096 / 0.11561	0.15009 / 0.11786
10	0.14661 / 0.10732	0.14652 / 0.11013	0.14610 / 0.11461	0.14756 / 0.11444
100	0.13183 / 0.10598*	0.13229 / 0.10807*	0.13160 / 0.10867*	0.13475 / 0.11010
1000	0.11196 / 0.11012	0.11175 / 0.10940	0.11236 / 0.11047	0.11195 / 0.10993*

Table S1c. Atlantic to Pacific, window-specific construction.

Penalty	M0	Mphase	Mcalendar	M1
0.1	0.12453 / 0.13163	0.12011 / 0.14304	0.13886 / 0.14083	0.12760 / 0.15208
1	0.11987 / 0.13019	0.11467 / 0.13792	0.13341 / 0.13947	0.11757 / 0.14703
10	0.11127 / 0.12928	0.10692 / 0.13404	0.11824 / 0.13750	0.10682 / 0.13981
100	0.10151 / 0.12193	0.10077 / 0.12318	0.10380 / 0.12425	0.10188 / 0.12499
1000	0.10129 / 0.12141*	0.09583 / 0.11998*	0.10085 / 0.12156*	0.09547 / 0.12054*

Table S1d. Atlantic to Pacific, fixed historical construction.

Penalty	M0	Mphase	Mcalendar	M1
0.1	0.12539 / 0.13241	0.12300 / 0.14236	0.14156 / 0.14061	0.13125 / 0.15185
1	0.12042 / 0.13144	0.11615 / 0.13812	0.13532 / 0.14024	0.11957 / 0.14722
10	0.11127 / 0.13112	0.10673 / 0.13545	0.11901 / 0.13900	0.10661 / 0.14087
100	0.10086 / 0.12338	0.09984 / 0.12455	0.10352 / 0.12550	0.10077 / 0.12616
1000	0.10146 / 0.12178*	0.09601 / 0.12044*	0.10104 / 0.12188*	0.09563 / 0.12088*

Table S1e. Pacific to Atlantic, window-specific construction.

Penalty	M0	Mphase	Mcalendar	M1
0.1	0.21806 / 0.10598	0.18974 / 0.10903	0.20432 / 0.12431	0.19972 / 0.11596
1	0.18280 / 0.10817	0.16830 / 0.11049	0.16925 / 0.11947	0.17174 / 0.11247
10	0.17980 / 0.10630	0.17187 / 0.10871	0.16767 / 0.11160	0.17427 / 0.11062
100	0.15025 / 0.10073*	0.14923 / 0.10069*	0.13794 / 0.10012*	0.14930 / 0.10248*
1000	0.10657 / 0.10884	0.10657 / 0.10771	0.10573 / 0.10823	0.10631 / 0.10709

Table S1f. Pacific to Atlantic, fixed historical construction.

Penalty	M0	Mphase	Mcalendar	M1
0.1	0.21553 / 0.10532	0.18918 / 0.10832	0.20183 / 0.12436	0.19532 / 0.11854
1	0.17884 / 0.10693	0.16243 / 0.11023	0.16658 / 0.11910	0.16317 / 0.11384
10	0.17750 / 0.10627	0.16915 / 0.10939	0.16601 / 0.11104	0.17096 / 0.11150
100	0.14937 / 0.10059*	0.14831 / 0.10106*	0.13655 / 0.09991*	0.14853 / 0.10291*
1000	0.10632 / 0.10848	0.10634 / 0.10750	0.10537 / 0.10790	0.10613 / 0.10691

S2 Original ecological result and observation support

Of 1296 candidate annual windows, 693 meet annual support and 666 also meet the seasonal-reference requirement. There are 367 development and 274 evaluation windows, including 60 and 18 zero-heatwave years; 25 crossing windows are excluded. Marginal support retains 211, 77 and 76 evaluation cases. A separate joint-nearest-neighbor screen retains 199, 61 and 84, with 185, 58 and 60 passing both screens. The primary population is not retrospectively replaced by that screen. No eligible annual window exists at 55°N.

Table S2. Original recorded criterion with original model-specific penalties. Bands are conditional and uncalibrated.

Scenario	Comparator	Cases	M1 / comparator MAE	Gain	Gain band	Condition met
Pooled	M0	211	0.1358 / 0.1327	-2.39%	[-7.22%, 0.43%]	No
Pooled	Mphase	211	0.1358 / 0.1330	-2.16%	[-5.58%, -0.03%]	No

Scenario	Comparator	Cases	M1 / comparator MAE	Gain	Gain band	Condition met
Pooled	Mcalendar	211	0.1358 / 0.1324	-2.64%	[-7.61%, 1.37%]	No
Atlantic to Pacific	M0	77	0.0955 / 0.1013	5.74%	[-1.56%, 20.87%]	No
Atlantic to Pacific	Mphase	77	0.0955 / 0.0958	0.37%	[-0.31%, 1.92%]	No
Atlantic to Pacific	Mcalendar	77	0.0955 / 0.1008	5.33%	[-1.63%, 19.17%]	Yes
Pacific to Atlantic	M0	76	0.1493 / 0.1503	0.63%	[-4.12%, 5.03%]	No
Pacific to Atlantic	Mphase	76	0.1493 / 0.1492	-0.04%	[-1.17%, 1.39%]	No
Pacific to Atlantic	Mcalendar	76	0.1493 / 0.1379	-8.24%	[-20.37%, -0.32%]	No

The criterion and results coexist in initial commit `4fd57a8351c4f7e8f70399a761a18b957d86b8dd` (7 October 2026, 20:58:57 −04:00). Accessible history contains no earlier timestamped protocol demonstrating that the criterion was fixed before evaluation was inspected. A source-code comment asserting earlier specification is not independent chronological evidence.

S3 Fold variability and hybrid reference controls

The two near-optimal M1 penalties exchange order after the historical geometry change. The original 1000-minus-100 fold differences are +0.007511, −0.000293, −0.007859 and +0.003633, on 82, 103, 103 and 79 validation cases. Different folds favor different penalties. The pooled original gap is 0.000172316; the changed gap is −0.000163201.

Table S3. Pooled M1 fold MAEs and heuristic SE. All models and penalties are retained in the machine-readable fold tables.

Construction	Penalty	Fold 1	Fold 2	Fold 3	Fold 4	Heuristic SE
Window-specific	0.1	0.12706	0.09829	0.13366	0.12426	0.00824
Window-specific	1	0.12365	0.09714	0.12889	0.12629	0.00776
Window-specific	10	0.11919	0.09417	0.11882	0.12727	0.00739
Window-specific	100	0.11674	0.09187	0.10776	0.12779	0.00764
Window-specific	1000	0.12425	0.09158	0.09990	0.13143	0.00955
Fixed historical	0.1	0.12706	0.10030	0.12577	0.12666	0.00685
Fixed historical	1	0.12405	0.09867	0.12361	0.12894	0.00708
Fixed historical	10	0.11978	0.09543	0.11760	0.12956	0.00737

Construction	Penalty	Fold 1	Fold 2	Fold 3	Fold 4	Heuristic SE
Fixed historical	100	0.11723	0.09311	0.10777	0.12786	0.00742
Fixed historical	1000	0.12455	0.09244	0.09929	0.13144	0.00949

Table S4. Retrospective one-standard-error rule. Its dispersion estimate is heuristic under the existing dependence and shared calibration.

Scenario	Construction	Model	Minimum alpha	One SE alpha	Heuristic SE	One SE MAE
Pooled	Window-specific	M0	100	1000	0.00634	0.11211
Pooled	Window-specific	Mphase	100	1000	0.00644	0.11193
Pooled	Window-specific	Mcalendar	100	1000	0.00753	0.11248
Pooled	Window-specific	M1	100	1000	0.00764	0.11214
Pooled	Fixed historical	M0	100	1000	0.00625	0.11196
Pooled	Fixed historical	Mphase	100	1000	0.00625	0.11175
Pooled	Fixed historical	Mcalendar	100	1000	0.00761	0.11236
Pooled	Fixed historical	M1	1000	1000	0.00949	0.11195
Atlantic to Pacific	Window-specific	M0	1000	1000	0.01505	0.10129
Atlantic to Pacific	Window-specific	Mphase	1000	1000	0.01484	0.09583
Atlantic to Pacific	Window-specific	Mcalendar	1000	1000	0.01525	0.10085
Atlantic to Pacific	Window-specific	M1	1000	1000	0.01512	0.09547
Atlantic to Pacific	Fixed historical	M0	1000	1000	0.01489	0.10146
Atlantic to Pacific	Fixed historical	Mphase	1000	1000	0.01467	0.09601
Atlantic to Pacific	Fixed historical	Mcalendar	1000	1000	0.01513	0.10104
Atlantic to Pacific	Fixed historical	M1	1000	1000	0.01487	0.09563
Pacific to Atlantic	Window-specific	M0	100	1000	0.00829	0.10657
Pacific to Atlantic	Window-specific	Mphase	100	1000	0.00874	0.10657
Pacific to Atlantic	Window-specific	Mcalendar	100	1000	0.00953	0.10573

Scenario	Construction	Model	Minimum alpha	One SE alpha	Heuristic SE	One SE MAE
Pacific to Atlantic	Window-specific	M1	100	1000	0.00938	0.10631
Pacific to Atlantic	Fixed historical	M0	100	1000	0.00911	0.10632
Pacific to Atlantic	Fixed historical	Mphase	100	1000	0.00938	0.10634
Pacific to Atlantic	Fixed historical	Mcalendar	100	1000	0.01029	0.10537
Pacific to Atlantic	Fixed historical	M1	100	1000	0.01003	0.10613

Table S5. Controlled historical substitutions on the original pooled evaluation cases. Gains here use the same original M0(100), making the comparator explicit.

Substitution	Selected alpha	MAE	EDF	Gain over original M0
Original	100	0.135845	12.480	-2.39%
Response only	100	0.135249	12.480	-1.94%
Predictors only	100	0.135215	12.468	-1.92%
Response and predictors	1000	0.111952	5.250	15.62%

The historical response changes by mean absolute 0.001402 and maximum 0.10505 under the full geometry change; the maximum boundary shift is 225 days. Fixed-penalty response and predictor substitutions have small pooled error effects, while joint substitution changes the selected penalty. None of these comparisons independently calibrates the constructed outcome.

S4 Existing variants and their actual complexity

All 400 development-year bootstrap draws pass in pooled and Atlantic-to-Pacific evaluation; 398 pass in Pacific-to-Atlantic. Pooled M1 selects 1000 in 62.25% and 65.50% of accepted draws under window-specific and fixed historical geometry, compared with 21.0% and 26.5% for M0. These frequencies condition on the existing references and eligibility.

The following original variants retain their own supported cases, so changes in MAE across variants are not automatically same-population gains. The associated scientific table also reports common intersections for the thermal and model-variant sets. Raw-longitude transfer has no marginal geographic overlap and is excluded from these intersections. The phase encodings span the same unpenalized model space; individual standardization and ridge penalties make their predictions coding-dependent. A symmetric contrast basis uses common within-group scales and is invariant to orthogonal rotations within those groups.

Table S6a. Pooled original variant comparisons.

Variant	Cases	M1 alpha / EDF	M0 alpha / EDF	M1 / M0 MAE	Gain
Original	211	100 / 12.48	100 / 9.96	0.1358 / 0.1327	-2.39%
Omit pre-bloom	211	100 / 12.37	100 / 9.96	0.1361 / 0.1327	-2.58%

Variant	Cases	M1 alpha / EDF	M0 alpha / EDF	M1 / M0 MAE	Gain
Omit rising	211	100 / 12.39	100 / 9.96	0.1344 / 0.1327	-1.28%
Omit declining	211	100 / 12.12	100 / 9.96	0.1357 / 0.1327	-2.25%
Symmetric phase contrasts	211	100 / 12.82	100 / 9.96	0.1367 / 0.1327	-3.01%
1991–2020 baseline	241	1000 / 5.23	100 / 9.94	0.1102 / 0.1271	13.29%
Detrended SST	257	100 / 12.54	1 / 15.79	0.1259 / 0.1439	12.51%
No heatwave-gap joining	212	100 / 12.48	100 / 9.95	0.1358 / 0.1329	-2.21%
0–50 m nitrate	218	100 / 12.50	100 / 10.02	0.1349 / 0.1328	-1.57%
Summer nitrate	218	100 / 12.49	100 / 10.05	0.1326 / 0.1322	-0.32%
Coverage covariates	211	1000 / 5.62	100 / 11.06	0.1128 / 0.1321	14.58%
Quadratic trend	211	1000 / 5.51	100 / 10.71	0.1137 / 0.1569	27.50%
Raw longitude	211	1000 / 5.12	100 / 9.28	0.1121 / 0.1327	15.53%

Table S6b. Atlantic to Pacific original variant comparisons.

Variant	Cases	M1 alpha / EDF	M0 alpha / EDF	M1 / M0 MAE	Gain
Original	77	1000 / 4.02	1000 / 3.29	0.0955 / 0.1013	5.74%
Omit pre-bloom	77	1000 / 4.02	1000 / 3.29	0.0946 / 0.1013	6.57%
Omit rising	77	1000 / 4.01	1000 / 3.29	0.0946 / 0.1013	6.59%
Omit declining	77	1000 / 3.96	1000 / 3.29	0.1001 / 0.1013	1.15%
Symmetric phase contrasts	77	1000 / 4.10	1000 / 3.29	0.0993 / 0.1013	1.99%
1991–2020 baseline	98	1000 / 3.99	1000 / 3.28	0.0944 / 0.0995	5.09%
Detrended SST	107	1000 / 4.01	1000 / 3.27	0.1109 / 0.1156	4.12%
No heatwave-gap joining	78	1000 / 4.02	1000 / 3.29	0.0946 / 0.1000	5.42%
0–50 m nitrate	73	1000 / 4.00	1000 / 3.29	0.0994 / 0.1054	5.75%

Variant	Cases	M1 alpha / EDF	M0 alpha / EDF	M1 / M0 MAE	Gain
Summer nitrate	70	1000 / 4.06	1000 / 3.38	0.0927 / 0.0990	6.32%
Coverage covariates	77	1000 / 4.23	100 / 9.17	0.0959 / 0.1062	9.67%
Quadratic trend	77	1000 / 4.19	1000 / 3.47	0.1095 / 0.1157	5.32%

Table S6c. Pacific to Atlantic original variant comparisons.

Variant	Cases	M1 alpha / EDF	M0 alpha / EDF	M1 / M0 MAE	Gain
Original	76	100 / 8.43	100 / 7.20	0.1493 / 0.1503	0.63%
Omit pre-bloom	76	100 / 8.32	100 / 7.20	0.1462 / 0.1503	2.69%
Omit rising	76	100 / 8.35	100 / 7.20	0.1455 / 0.1503	3.16%
Omit declining	76	100 / 8.30	100 / 7.20	0.1459 / 0.1503	2.90%
Symmetric phase contrasts	76	100 / 8.73	100 / 7.20	0.1462 / 0.1503	2.73%
1991–2020 baseline	78	100 / 8.40	100 / 7.16	0.1272 / 0.1334	4.63%
Detrended SST	83	100 / 8.43	100 / 7.13	0.1339 / 0.1350	0.79%
No heatwave-gap joining	75	100 / 8.43	100 / 7.19	0.1496 / 0.1506	0.71%
0–50 m nitrate	90	100 / 8.75	100 / 7.47	0.1464 / 0.1474	0.64%
Summer nitrate	90	100 / 8.87	100 / 7.56	0.1468 / 0.1470	0.14%
Coverage covariates	76	100 / 9.16	100 / 7.93	0.1499 / 0.1509	0.68%
Quadratic trend	76	10 / 15.32	10 / 12.82	0.4986 / 0.5074	1.73%

Pooled gains under five phase encodings range from −3.01% to −1.28% on identical cases. These modest changes do not rescue the original pooled criterion. Detrended SST is distinct from deleting the prediction model's trend covariate: it changes heatwave construction and eligibility.

S5 Influence and explanatory sensitivities

All coefficient paths, year/basin errors, trend-removal fits, basin-indicator fits and the extended penalty grid are retained in the numerical tables. The basin indicator is penalized; it is constant in single-basin training and hence cannot identify a new destination-basin offset. Dropping a trend refits the remaining correlated predictors and does not causally remove time.

Table S7. Pooled original-construction deletion ranges. These are influence ranges, not confidence intervals.

Contrast	Deleted group type	Minimum cases	MAE difference range
M1 1000 minus 100	Spatial Block	193	[-0.02696, -0.02127]
M1 1000 minus 100	Temporal Block	137	[-0.03155, -0.01730]
M1 1000 minus 100	Year	185	[-0.02665, -0.01981]
M0 1000 minus 100	Spatial Block	193	[-0.02393, -0.01760]
M0 1000 minus 100	Temporal Block	137	[-0.02710, -0.01553]
M0 1000 minus 100	Year	185	[-0.02309, -0.01737]
M1 minus M0 at 1000	Spatial Block	193	[-0.00052, 0.00069]
M1 minus M0 at 1000	Temporal Block	137	[-0.00025, 0.00048]
M1 minus M0 at 1000	Year	185	[-0.00041, 0.00090]
M1 minus Mphase at 1000	Spatial Block	193	[-0.00020, 0.00035]
M1 minus Mphase at 1000	Temporal Block	137	[-0.00010, 0.00065]
M1 minus Mphase at 1000	Year	185	[-0.00024, 0.00038]

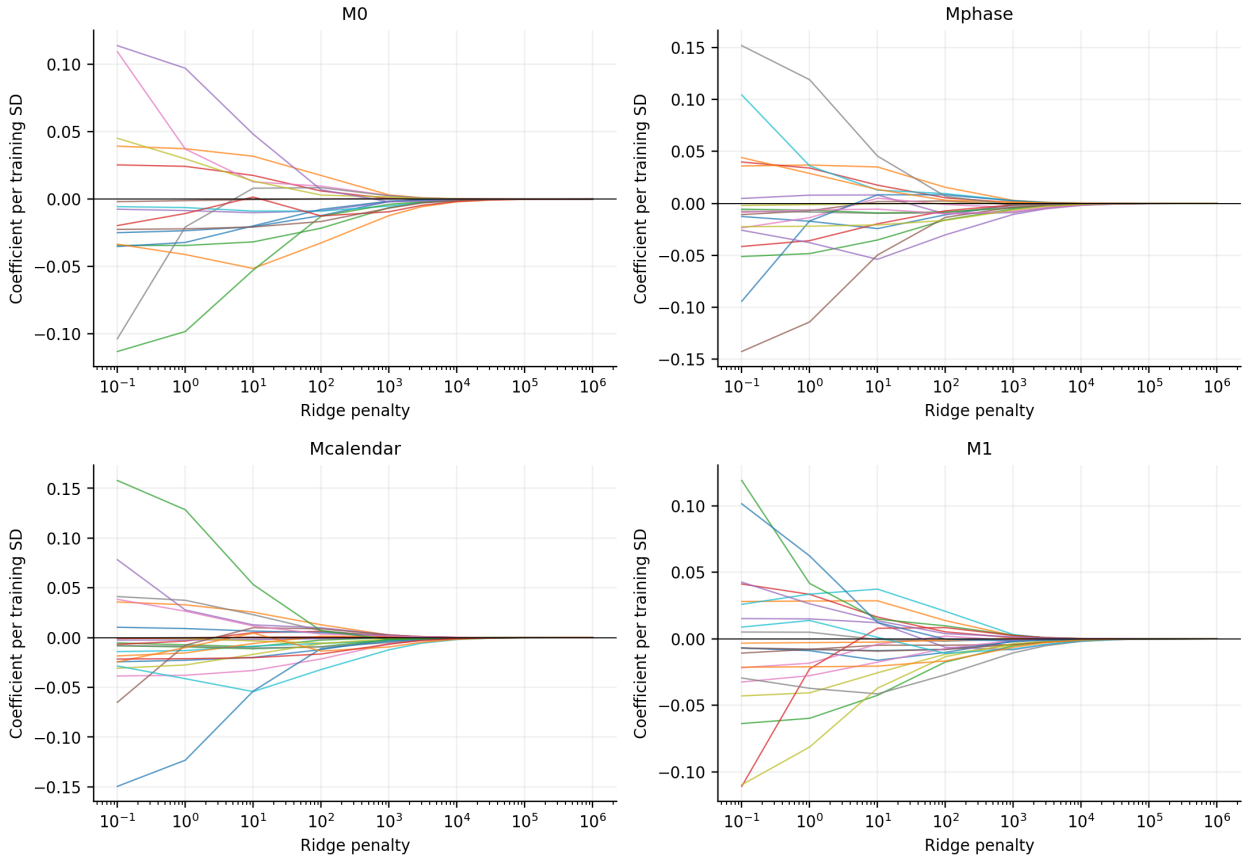


Figure S1. Standardized coefficient paths for every original-design predictor, pooled original construction. Each line is one coefficient; these paths show joint attenuation, not causal attribution. The accompanying table identifies each feature and gives original-unit coefficients as well.

The all-target EDF uncertainty analysis retains 108 contrasts: six EDF targets, three comparators, two constructions and three scenarios. All Atlantic-to-Pacific primary bands span zero. Pacific-to-Atlantic has some favorable M1–M0 and M1–Mphase primary bands at intermediate EDF, but Mcalendar is better at those settings. The original reverse-transfer M1 at EDF2 has MAE 0.103751, slightly below zero-null 0.104382; the original-grid null result should not be extended to every post

hoc EDF fit. No EDF target is selected as a replacement forecast. Complete bands, partition counts and deletion ranges are in the EDF tables.

S6 Separate reference calibration

The original attempt to separate calibration and development uses 1998–2007 for the reference and 2008–2013 for development. It retains the minimum reference-year, seasonality, observation and tuning-fold requirements. The fixed comparison contains 11 Atlantic and three Pacific tiles. Pooled training has 70 observations across only two nominal temporal groups; Atlantic-to-Pacific has 55 training observations and Pacific-to-Atlantic only 15. No scenario passes the required development fitting conditions. This feasibility result prevents claiming an independent-calibration replication. It does not imply that no larger dataset or redesigned prospective study could support one. The existing reference-component substitutions, population counts and failed-fit status remain in the scientific outputs.

S7 Coverage simulation retained as a limited stress test

This original simulation is not evidence for empirical interval coverage. It preserves evaluation group geometry and generates one common outcome for two fixed predictors, with spatial/temporal random effects, heteroscedasticity or persistent annual errors. The predictions lie on opposite sides of the simulated mean. Each setting uses 400 datasets and 1000 bootstrap draws. The complete simulation, including its unfavorable error-structure comparison, is retained to make its limits inspectable.

Table S8. Simulation coverage of nominal 95% gain bands and Monte Carlo Wilson intervals. Some scenarios under-cover; others reach 100%.

Simulation	True gain	Pooled	Atlantic to Pacific	Pacific to Atlantic
independent rows	0%	99.8% [98.6%, 100.0%]	98.8% [97.1%, 99.5%]	98.5% [96.8%, 99.3%]
independent rows	10%	100.0% [99.0%, 100.0%]	98.2% [96.4%, 99.1%]	98.0% [96.1%, 99.0%]
strong temporal blocks	0%	81.5% [77.4%, 85.0%]	84.0% [80.1%, 87.3%]	82.2% [78.2%, 85.7%]
strong temporal blocks	10%	83.2% [79.3%, 86.6%]	87.2% [83.6%, 90.2%]	80.0% [75.8%, 83.6%]
strong shared space	0%	93.5% [90.6%, 95.5%]	85.0% [81.2%, 88.2%]	87.2% [83.6%, 90.2%]
strong shared space	10%	91.5% [88.4%, 93.9%]	90.0% [86.7%, 92.6%]	87.8% [84.2%, 90.6%]
heteroscedastic crossed	0%	86.8% [83.1%, 89.7%]	92.2% [89.2%, 94.5%]	93.5% [90.6%, 95.5%]
heteroscedastic crossed	10%	90.8% [87.5%, 93.2%]	91.5% [88.4%, 93.9%]	89.8% [86.4%, 92.4%]
persistent AR years	0%	58.5% [53.6%, 63.2%]	58.5% [53.6%, 63.2%]	57.8% [52.9%, 62.5%]
persistent AR years	10%	51.0% [46.1%, 55.9%]	59.2% [54.4%, 64.0%]	59.8% [54.9%, 64.4%]

Simulated median normalized prediction separation spans 1.55–1.95, compared with 0.07–0.12 empirically for the original selected M1–M0 comparisons. Simulated paired absolute-loss correlations are approximately -0.75 to -0.50, versus $+0.97$ to $+0.99$ empirically. Preserving group geometry therefore does not reproduce the relevant empirical error structure. A separate arbitrary paired-

lognormal-loss exercise is retained in the original outputs, with coverage 51.5–99.8%; it likewise cannot validate the empirical bands.

S8 Preserved secondary ecological analyses

These analyses preserve the original investigation and negative results; they are not used to select the revised central claim. H1 proposes negative annual responses in low-nitrate 25/35°N strata and positive responses in high-nitrate 45/55°N strata. None of seven recorded expected-sign summaries has a nominal band wholly in the expected direction, and the 55°N observations are absent. Strata are not redefined after observing support failures.

H2 relates calendar-control-corrected absolute chlorophyll anomaly to heatwave intensity and log-base-two duration relative to ten days, including quadratic terms, their interaction, nitrate interactions, calendar, geography, trend and coverage. Calendar-matched heatwave-free controls in neighboring years require observed support and clean 16-day margins. Earlier and later controls receive equal weight; each absolute control anomaly is computed before averaging. Reported duration derivatives are local slopes, not exact finite doubling effects.

H3 relates observed bloom onset and duration to thermal exposure before reference onset. A 17-day smoother and peak search from 120 days before to 150 days after the reference peak define own-amplitude, fixed-reference-amplitude and cumulative-excess endpoints. Threshold crossings require 16-day persistence, observations on both sides within eight days, and two distinct composites. Cumulative 10–90% endpoints use the same support requirement. Exposure before reference onset can occur after observed onset: this happens in 14.85% of 357 supported positive-exposure years. A strictly pre-observed sensitivity uses an outcome-dependent exposure window. These associations cannot establish temporal causality.

For absolute anomaly minus matched-control absolute anomaly, the H2 intensity and local log-duration estimates are −0.029 [−0.094, 0.041] and +0.007 [−0.017, 0.026], on 2101 observations. H3 onset estimates per 100 °C-days are −3.35 [−21.68, 8.81] days for own amplitude (572 observations), +3.24 [−4.85, 11.98] for fixed amplitude (598), and −1.18 [−5.23, 3.89] for cumulative excess (637). Corresponding duration estimates are −0.14 [−13.76, 14.17], −8.64 [−22.90, 7.30], and +0.71 [−6.01, 7.74]. All bands and false-discovery adjustments remain exploratory and unvalidated.

For annual accounting, the common reference denominator gives $Q = Q_{event} + Q_{outside} = D_+ - D_-$. Among 492 of 693 eligible windows with negative heatwave-day contribution, 187 (38.0%) have positive outside-event contribution and 148 (30.1%) have nonnegative annual Q. These are conditional descriptive counts, not independent prevalence or proof of ecological compensation. Of 253,133 represented days, 8228 (3.25%) are reconstructed. Zero-heatwave years remain in the accounting. Within-three-year-block exposure reassignment leaves 41.1–42.6% of evaluation rows unchanged on average; these are restricted sensitivity controls, not randomized null tests. Injected-effect exercises omit the complete ecological conjunction and cannot establish its power.

S9 Targeted penalty-resolution and reference-boundary diagnostics

These diagnostics were specified retrospectively after the original results were inspected. The penalty-resolution analysis uses development observations only, with 63 fixed penalties: 0.1, 1, and 61 log-spaced points from 10 through 10000 at 0.05-decade spacing. The original 100 and 1000 anchors are exact. Models M0/M1, both constructions, and designs with/without trend are retained under four policies. All-blocked uses all four original folds (367 validation rows). Common-blocked, earlier-only and weight-normalized earlier-only use the same last three validation blocks (285 rows). The first block cannot support earlier-only fitting and is not replaced. The original validation rows comprise 206 interior, 82 earliest-block backward and 79 last-block forward cases. The common blocks are 2002–2005, 2006–2009 and 2010–2012; the infeasible earlier-only block is 1998–2001.

Earlier-only training retains years strictly below the first validation year minus one. Weight-normalized earlier-only training multiplies every training weight by the corresponding blocked/earlier-only row-count ratio: 216/60, 211/159 and 262/262. Validation losses remain unweighted and pooled by their identical case counts. This is equivalent to unweighted ridge at penalty multiplied by the earlier-only/blocked count ratio, with the same training standardization; it controls the summed-loss scale, not information content. Full curves, fold identities, losses, fitted EDF, trend coefficients, validation-year losses and fixed-100/1000 predictions are retained. The sampled 1%-of-minimum ranges are descriptive; no continuous optimum, coverage or replacement model is claimed. Cross-construction development scores do not share identical historical outcomes, unlike within-construction chronology comparisons.

Table S9. All tested dense-grid development minima. Scores are historical validation MAEs; no later-year score was calculated.

Geometry	Design	Chronology	M0 alpha	M1 alpha	M1 CV MAE
Window-specific	With trend	All four blocked	112.20	398.11	0.108471
Window-specific	With trend	Common three blocked	112.20	501.19	0.104947
Window-specific	With trend	Earlier only	125.89	354.81	0.107781
Window-specific	With trend	Earlier, weight normalized	199.53	562.34	0.109010
Window-specific	No trend	All four blocked	177.83	501.19	0.111039
Window-specific	No trend	Common three blocked	223.87	630.96	0.107135
Window-specific	No trend	Earlier only	141.25	446.68	0.110362
Window-specific	No trend	Earlier, weight normalized	281.84	707.95	0.111250
Fixed historical	With trend	All four blocked	112.20	398.11	0.108832
Fixed historical	With trend	Common three blocked	112.20	446.68	0.105347
Fixed historical	With trend	Earlier only	125.89	446.68	0.108035
Fixed historical	With trend	Earlier, weight normalized	316.23	707.95	0.109342
Fixed historical	No trend	All four blocked	223.87	562.34	0.111406
Fixed historical	No trend	Common three blocked	223.87	891.25	0.107394
Fixed historical	No trend	Earlier only	199.53	501.19	0.110506
Fixed historical	No trend	Earlier, weight normalized	316.23	891.25	0.111465

Boundary shifts compare every original eligible seasonal development identity with its fixed-historical counterpart. Actual-date differences retain leap days and the original start-year label. The signed shortest circular phase difference is $((a_{fixed} - a_{window} + 182.5) \bmod 365) - 182.5$. Extreme cases are selected before curve inspection as all absolute actual shifts of at least 90 days, plus maxima of actual

and circular displacement including ties; this yields ten cases in five tiles. Full and target-excluded curves are reconstructed from 3680 historical composites with the original reference fitting and exclusion rules. Cyclic local minima are matched within 30 phase days; numerical ties use tolerance $10^{-10}\max(1, |c_{min}|)$. No selected global minimum has a numerical tie. Each curve has a competing local minimum near the other curve's global anchor whose depth ranking reverses. These matching rules describe fitted curves and do not identify ecological causes.

Table S10. Distribution across all 367 paired historical windows.

Quantity	Median	90th percentile	95th percentile	Maximum
Absolute actual shift (days)	2.0	4.0	6.0	225.0
Absolute circular shift (phase days)	2.0	4.0	6.0	145.0
Absolute response change	0.000304	0.001457	0.002361	0.105054

Table S11. Every selected extreme boundary case. Signs are fixed-historical minus window-specific geometry.

Tile	Year	Actual days	Circular phase days	Response change
ATL 25N 26W	2009	-92	-92	0.042573
ATL 25N 26W	2010	-93	-93	0.000417
ATL 45N 20W	2004	225	-141	-0.105054
ATL 45N 20W	2005	224	-141	0.037855
PAC 25N 140W	2009	145	145	-0.011980
PAC 25N 140W	2010	140	140	-0.026758
PAC 25N 170W	2002	-122	-122	-0.015289
PAC 35N 140W	1999	-123	-123	-0.005706
PAC 35N 140W	2008	-121	-121	0.077809
PAC 35N 140W	2009	-122	-122	-0.008708

Figure 3 in the main text shows reconstructed seasonal curves for the largest actual-date and shortest-circular displacements. All ten extreme cases and their local minima are retained in the numerical evidence.

S10 Detailed exposure definitions

Let $c_j = C_0(j)$ on the 365-day phase grid $j = 0, \ldots, 364$, with 1 January at zero. Choose the first minimum a and first maximum p in that calendar order, and set $h = \min_j c_j + 0.2(\max_j c_j - \min_j c_j)$. With $z_u = c_{(a+u) \bmod 365}$ and $p_u = (p - a) \bmod 365$, reference onset and termination search integer $u \in \{0, \ldots, 364\}$ and are

$$u_s = 1 + \max\{u \le p_u : z_u < h\}, \qquad u_e = \min\{u \ge p_u : z_u < h\}.$$

The defaults are $u_s = 0$ or $u_e = 364$ if the respective set is empty. Set $s = (a + u_s) \bmod 365$ and $e = (a + u_e) \bmod 365$. Equality to the threshold remains inside the crossing interval; termination is the first strictly below-threshold phase after the peak. Exact global-extremum ties use the earliest calendar index, without an ecological tie-breaker. The amplitude and separated-secondary-peak requirements above screen eligibility; they do not replace this 20%-amplitude boundary rule. These reference landmarks differ from the observed, persistence-based phenology outcomes in Supplement S8.

For a date t, let $d(t)$ be its 365-calendar phase, with 28 February at 58, 29 February at 58.5 and 1 March at 59. Define $x = (d(t) - s) \bmod 365$, $P = (p - s) \bmod 365$ and $E = (e - s) \bmod 365$.

Start with all days in the remaining phase; assign pre-bloom when $x \geq 275$, then rising when $0 \leq x \leq P$, then declining when $P < x \leq E$, in that order. Thus onset and peak belong to rising, the first below-threshold termination belongs to declining, and rising/declining overwrite any nominal pre-bloom overlap. Every date has one phase. Annual windows use actual dates, including leap days, from the boundary in calendar year y up to, but excluding, that boundary in $y + 1$.

Let I_t indicate detector-flagged heatwave days and $D_t = I_t \max(T_t - T_{\text{clim},t}, 0)$ denote daily positive excess-temperature dose. Phase dose is $\sum_{t \in W} D_t \mathbf{1}\{t \text{ in phase } b\}$. Calendar harmonics are

$$S_k = \sum_{t \in W} D_t \sin\left(\frac{2\pi k d(t)}{365}\right), \qquad C_k = \sum_{t \in W} D_t \cos\left(\frac{2\pi k d(t)}{365}\right), \quad k = 1, 2, 3.$$

These are unnormalized signed dose moments in °C-days, retaining exposure magnitude rather than estimating mean timing conditional on exposure. Heatwave days equal $\sum I_t$; mean intensity is $\sum I_t(T_t - T_{\text{clim},t}) / \sum I_t$, including flagged joined-gap days. When there are no heatwave days, mean intensity is defined as zero, and all total, phase and calendar dose quantities are zero.

S11 Additional selection complexity and prediction diagnostics

Selection and uncertainty procedures

For a retrospective one-standard-error sensitivity, let w_k be a fold's fraction of validation rows, L_k its MAE, and $\bar{L} = \sum_k w_k L_k$. We calculate

$$s_w^2 = \frac{\sum_k w_k (L_k - \bar{L})^2}{1 - \sum_k w_k^2}, \qquad SE_{\text{heur}} = s_w \sqrt{\sum_k w_k^2}.$$

The rule chooses the largest original-grid penalty with loss no greater than the minimum plus this heuristic SE at the minimum (Hastie, Tibshirani, and Friedman 2009). Overlapping training samples, dependence and shared reference fitting prevent this fold statistic from being a calibrated uncertainty estimate (Bengio and Grandvalet 2004; Varoquaux 2018). A small observed loss gap is not proof that selection is arbitrary.

Selection sensitivity uses every boundary origin for three-, four- and five-year validation blocks, giving 12 partitions, and 400 bootstrap samples of development years per scenario. Resampled copies of a year remain grouped through fitting and validation. Training weights are normalized to the corresponding original row count to retain the ridge penalty scale. References and eligibility are held fixed. Rejected draws are recorded, not replaced. These are conditional procedural perturbations, not an end-to-end sampling distribution; the bootstrap MAE distribution also reflects refitting, not just penalty switches.

We examine coefficient paths, year and basin errors, refits without the linear trend, and a pooled basin indicator. We also exclude every evaluation window containing any 2023–2024 day, leaving 174 pooled cases. A clearly post hoc grid adds penalties 3000, 10^4, 3×10^4, 10^5 and 10^6. These evaluations describe the shrinkage path; they do not select a new recommended model. To separate penalty from model complexity, each design is also fitted at EDF targets 2, 4, 6, 8, 10 and 14. The penalty achieving each target is calculated from the training design alone. All targets and comparisons are retained.

Paired uncertainty diagnostics keep fitted models and evaluation cases fixed. A two-way block bootstrap independently samples temporal groups and spatial groups with replacement, multiplies their case weights and computes a row-weighted paired MAE difference. The primary grouping has three-year temporal blocks and adjacent longitude pairs within basin and latitude. There are four temporal groups and 15, six and five spatial groups in the three scenarios. We use 10,000 draws, percentile 95% bands, and a display safeguard of at least 30 cases and four groups in each dimension.

Empty draws are excluded and counted. Alternative temporal widths 2–4 and spatial widths 1–3, with every origin, yield 54 partitions; 36 satisfy the safeguard. Deleting one year, temporal block or spatial block measures influence without refitting. These bands are nominal and conditional; the safeguard is not a coverage guarantee.

The original ecological criterion, H^*, requires in each scenario at least 10% gain over M0 with a positive lower resampling bound, a positive lower bound over Mphase, and nonnegative point gain over Mcalendar. The initial accessible repository commit on 7 October 2026 contains this criterion and completed results together. It does not establish that the criterion preceded examination of evaluation outcomes. We therefore call it the **original recorded criterion**, not a verified preregistered test.

Equal complexity and absolute skill

Equal-EDF comparisons must be read against the pooled calibrated-reference benchmark MAE of 0.116358. Under window-specific geometry, all four models are worse than zero at EDF 10 and 14. At EDF 8, M0, Mphase and M1 are worse, while Mcalendar remains better (MAE 0.115021). At EDF 6, M0 is worse than zero, but Mphase (0.114692), M1 and Mcalendar are better. Higher relative performance than another fitted model therefore need not imply useful skill beyond that reference for annual anomalies.

Table S12. Pooled equal-EDF comparisons under window-specific geometry. All targets were retained; none was selected by evaluation error. Mphase shows the point comparator for the added phase-dose–nitrate interactions. Bands are conditional nominal 95% bands for M1 minus M0.

EDF	M0 MAE	Mphase MAE	M1 MAE	Mcalendar MAE	M1 minus M0 band
2	0.113447	0.112818	0.112940	0.114478	[-0.00201, 0.00039]
4	0.111684	0.110765	0.110345	0.111712	[-0.00418, 0.00087]
6	0.116650	0.114692	0.113692	0.112375	[-0.00815, 0.00114]
8	0.124176	0.121275	0.119695	0.115021	[-0.01081, 0.00075]
10	0.132861	0.128477	0.127126	0.119280	[-0.01312, 0.00021]
14	0.147451	0.142032	0.140474	0.129675	[-0.01585, -0.00017]

Pooled M1 has lower MAE than M0 at all six declared EDF targets, with window-specific gains of 0.45–4.73%; these point differences retain their direction after every individual year, temporal-block and spatial-block deletion under both constructions. Nevertheless, the primary pooled M1–M0 bands span zero at EDF 2–10, and all pooled M1–Mphase primary bands span zero. At EDF 14, M1–M0 is -0.006977 with nominal band $[-0.015846, -0.000174]$, but only 14 of 36 displayed dependence partitions exclude zero under each construction. These reuse the same cases and describe sensitivity rather than independent confirmations.

Mcalendar has lower point MAE than M1 at EDF 6, 8, 10 and 14. The M1-minus-Mcalendar primary bands are wholly positive at EDF 10 and 14; at 14 the difference is +0.010799 [0.002475, 0.022586]. Equal EDF fixes the total smoother trace without equating shrinkage directions. The results preserve uncertainty about the incremental phase-dose–nitrate terms and give no basis for

selecting a generally superior phase model. Every target remains reported without choosing an evaluation-preferred winner.

Accounting for the original headline comparison

With window-specific geometry, selected M1 at penalty 100 has MAE 0.135845 versus 0.132673 for M0 at 100, a gain of −2.39%. Fixed historical geometry selects M1 at 1000, with MAE 0.111952 and a +15.62% gain against the unchanged original M0 comparator. Its selected M0 remains at 100, with MAE 0.131828; the within-construction gain is 15.08%. These are correct realized comparisons whose interpretation depends on the near-tied coarse-grid selection described in the main text.

The complete +15.62% headline difference follows the chosen sequential path from window-specific M0(100), through window-specific M0(1000) and M1(1000), to fixed-historical M1(1000). Its MAE reduction is

$$0.020562 - 0.000031 + 0.000191 \approx 0.020721.$$

The three terms represent, in order, the baseline penalty change, the phase-block addition under window-specific geometry, and the reference change at M1(1000).

The displayed terms are rounded; unrounded terms close exactly. This path shows a small fixed-penalty reference effect relative to baseline shrinkage, alongside the reference's larger consequence through discrete selection. It is an accounting identity along a chosen path, not a unique allocation among predictors, penalty and reference, or a causal decomposition of ecological processes. Nor would the original exact-minimum selector have chosen M0(1000): its development MAE is 0.109974 versus 0.105259 at 100, with the same ordering under fixed historical geometry.

Paired differences and influence

Table S13. Pooled window-specific-geometry paired differences and conditional nominal 95% bands. Negative favors the first fit.

Comparison	MAE difference	Nominal band
M1 1000 minus 100	-0.023702	[-0.04996, -0.00468]
M0 1000 minus 100	-0.020562	[-0.04509, -0.00300]
M1 minus M0 at 1000	0.000031	[-0.00415, 0.00327]
M1 minus Mphase at 1000	0.000209	[-0.00122, 0.00261]

The pooled within-M1 penalty difference is −0.023702, with primary nominal band [−0.049957, −0.004680]. Its sign remains negative after deletion of each year, temporal block or spatial block, and all 36 displayed partition bands lie below zero under both constructions. M0 also improves, although some alternative partition bands cross zero. All displayed matched M1–M0 and M1–Mphase bands at 1000 span zero and their point signs can change after deletions. All 72 primary null-relative bands span zero. These conditional diagnostics separate the observed shrinkage improvement from uncertain incremental predictive value.

Trend year and basin diagnostics

At penalty 100, deleting the trend reduces original M0/M1 MAEs from 0.132673/0.135845 to 0.118759/0.121214. Between penalties 100 and 1000, the M0 trend coefficient changes from −0.003957 to −0.001593 per year, and M1 from −0.003956 to −0.001523. Other correlated coefficients also change (Figure S1). No-trend M1 still improves to 0.110235 at 1000, showing that the explicit trend is only part of the explanation. Adding a penalized basin indicator alone does not resolve the low-penalty deficit.

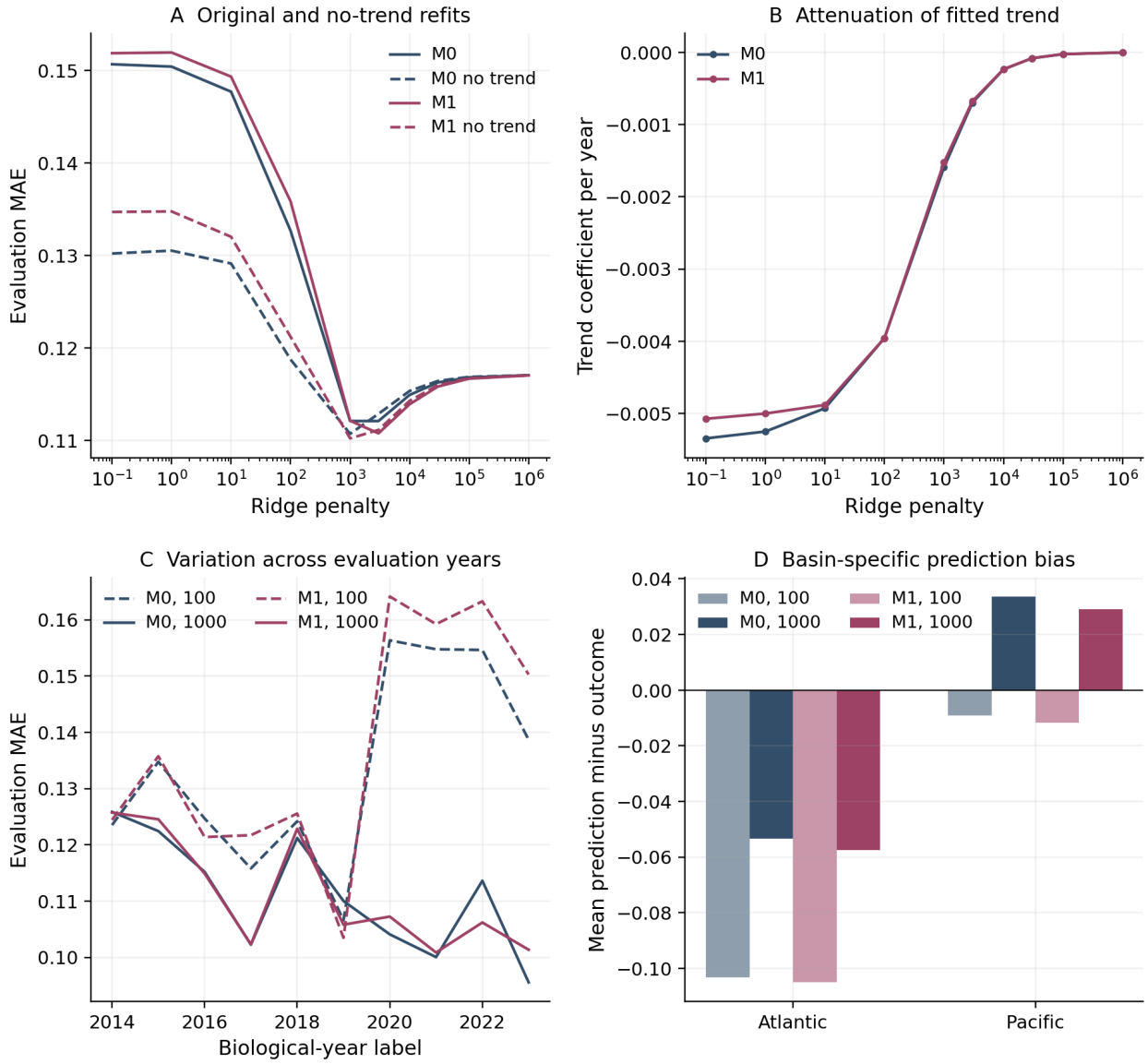


Figure S2. Pooled explanatory sensitivities. Panel A compares original and no-trend fits; B shows original-unit trend coefficients; C retains biological-year MAEs; D shows basin mean prediction-minus-observation bias. Most shrinkage benefit occurs in the 2020–2022 labels, and opposite-signed basin biases persist at penalty 1000. All refits are retrospective.

The gain is concentrated but not confined to the provisional 2023–2024 observations. On 174 cases containing no such days, fixed-fit M1 MAEs are 0.131130 at 100 and 0.113827 at 1000; M0 gives 0.129378 and 0.113351. On the extended penalty grid, fits approach the training-mean prediction; evaluation error does not fall indefinitely, and development selection for the original designs is unchanged. No evaluation minimum is used to recommend a penalty.

Chronology procedural stability and transfer

Removing the earliest validation block makes the coarse-grid M1 choice 1000 under both constructions, before restricting training to earlier years. On the remaining three common blocks, removing the trend worsens earlier-only M1 validation at both 100 and 1000, by approximately 0.0038 and 0.0017 without weight normalization. The trend therefore remains useful in these historical extrapolation fits. This qualifies a simple interpolation-versus-extrapolation explanation of later-year failure. References still use shared historical calibration, including years later than some validation blocks; this is conditional chronology sensitivity. Supplement S9 gives fold membership, training counts, weight normalization and dense-grid minima.

Selection sensitivity is scenario-specific (Table S14). Across 12 validation-block partitions, pooled M1 chooses 1000 in three under window-specific geometry and four under fixed historical geometry; M0 never does. Atlantic-to-Pacific M1 chooses 1000 in all 12 partitions under both constructions, while Pacific-to-Atlantic M1 does so in none. The year bootstrap and retrospective one-standard-error rule provide further procedural comparisons (Supplements S3–S4), without establishing calibrated selection probabilities or equality of competing losses.

Table S14. M1 selection sensitivity. Boundary counts summarize 12 alternative historical block partitions; bootstrap frequencies summarize accepted resamples of development years. They are different perturbations, not two estimates of one selection probability. MAE quantiles are descriptive 2.5th, 50th and 97.5th percentiles on the fixed later-year evaluation cases for each scenario after refitting each bootstrap sample; they are not development scores or confidence limits.

Scenario	Construction	Boundary count at 1000	Bootstrap at 1000	Evaluation MAE quantiles
Pooled	Window-specific	3/12	62.25%	0.1110 / 0.1139 / 0.1632
Pooled	Fixed historical	4/12	65.50%	0.1109 / 0.1135 / 0.1615
Atlantic to Pacific	Window-specific	12/12	85.50%	0.0895 / 0.0969 / 0.1317
Atlantic to Pacific	Fixed historical	12/12	88.50%	0.0892 / 0.0969 / 0.1309
Pacific to Atlantic	Window-specific	0/12	26.38%	0.1017 / 0.1448 / 0.2227
Pacific to Atlantic	Fixed historical	0/12	27.89%	0.1016 / 0.1436 / 0.2183

The existing analysis variants also differ: the alternative heatwave baseline, coverage-covariate and raw-longitude variants select pooled M1 at 1000, whereas detrended sea-surface temperature selects M1 at 100 and M0 at 1. Supplement S4 reports their penalties, EDF and evaluation populations; they are not interchangeable examples of one selection mechanism.

At penalty 1000, original Atlantic-to-Pacific M1 improves by 5.74% over M0 but only 0.375% over Mphase. Across phase encodings, the M1–M0 gain is 1.15–6.59%, including 1.99% with symmetric contrasts (Table S6b). Their unpenalized model space is shared but their scaled ridge penalties

differ. This direction-specific point result is therefore representation-dependent. Pacific-to-Atlantic does not confirm the original ecological criterion. Across all three scenarios, only one of the original criterion's nine comparator conditions is met: Atlantic-to-Pacific versus Mcalendar. The quadratic-trend reverse-transfer variant has particularly large MAEs (0.498557 for M1 and 0.507359 for M0), illustrating sensitivity of temporal extrapolation rather than a stable improvement.

S12 Observation support and information availability

The support audit uses half-open calendar intervals and composite-supported days before interpolation. A usable day is represented by a retained tile composite with at least 20% observed fraction and finite positive chlorophyll. An eight-day composite supplies one aggregate over eight nominal days; these are not eight independent acquisitions. Counts are summed within tiles, so equal dates in different tiles are distinct tile-days. Duplicate membership excess is total row-day membership minus the union. Adjacent retained labels differing by more than one year are reported separately; uncovered days inside a tile's overall envelope include attrition and must not be called boundary-induced gaps.

Table S15. Development observation support on the same 367 windows. Gaps use only the 329 consecutive-label pairs; missing labels are separately retained in the numerical evidence. A composite-supported tile-day is not an independent daily observation or a constant pixel footprint.

Support measure	Window-specific	Fixed historical
Calendar row-day memberships	134053	134052
Unique calendar tile-days	133212	134052
Duplicate calendar memberships	841	0
Unique usable-composite tile-days	127486	128276
Duplicate usable-composite memberships	810	0
Gaps between consecutive labels, calendar tile-days	1143	0
Gaps between consecutive labels, usable-composite tile-days	1095	0

Table S16. Attrition by basin, latitude, label-year period and actual split. Groupings are separate marginal summaries, not additive populations. Joint basin/latitude/period counts and exclusion reasons are retained in the numerical evidence.

Grouping	Stratum	Candidate	Annual support	Seasonal support
all	all	1296	693	666
basin	ATL	648	400	400
basin	PAC	648	293	266
lat	25	324	307	280
lat	35	324	296	296
lat	45	324	90	90
lat	55	324	0	0
period	1998-2005	384	193	185
period	2006-2013	384	216	207
period	2014-2024	528	284	274
split	development	720	383	367

Grouping	Stratum	Candidate	Annual support	Seasonal support
split	holdout	528	284	274
split	purged_boundary	48	26	25

Table S17. Inherited stricter-support analyses, newly summarized without model refitting. The 30% rule changes retained composites and Q; the 90% rule changes annual eligibility with Q unchanged. Both keep the original reference/geometry and do not enforce a common native-pixel footprint.

Requirement	Cohort	Original	Retained	95th percentile absolute Q change	Q sign changes
30% pixel coverage	Annual	693	659	0.013662	4
30% pixel coverage	Seasonal	666	634	0.013959	4
90% annual coverage	Annual	693	629	0.000000	0
90% annual coverage	Seasonal	666	605	0.000000	0

Among 666 seasonal windows, median observed-day and interval coverage are 0.9781 and 0.9787. Mean native-pixel coverage within a window has minimum 0.5198, median 0.8808 and maximum 0.9988. Full distributions by basin, latitude, period and split are retained. The inherited 30% pixel requirement retains 343 of 367 development and 266 of 274 later seasonal windows; its 95th percentile absolute Q change is 0.0140 overall, with four sign changes. The 90% annual-coverage rule retains 605 seasonal windows, with Q unchanged. These October sensitivities are newly summarized, not rerun or used for new model selection. They diagnose support dependence without establishing a common satellite footprint.

Table S18. Information availability in the implemented retrospective pipeline. "Target" refers to the window being constructed; "fold" to its held-out development block. Access to availability or an external climatology is distinct from fitting directly to later chlorophyll outcomes.

Component	Target and other validation-fold data	Evaluation-period access and interpretation
Concentration reference C0	Historical target calendar years y and y+1 excluded; other fold years retained	No 2014+ chlorophyll magnitudes fitted into C0; input eligibility inherits the all-year coverage denominator
Window-specific boundaries and landmarks	Same target-excluded reference; other fold years retained	Later landmarks use the full 1998–2013 curve
Fixed historical boundaries and landmarks	Full 1998–2013 geometry includes historical target and fold years; concentration denominator remains target-excluded	Same later geometry and cases as window-specific construction

Component	Target and other validation-fold data	Evaluation-period access and interpretation
Eligibility and seasonality	Target coverage, gaps and support determine inclusion; no fold-wide reconstruction	Later availability determines inclusion; changed historical windows retain the original seasonal cohort
Satellite footprint and observed fraction	Valid pixels vary per composite; denominator shared across folds	Empirical mask unions downloaded 1998–2024 retrievals, so later availability can affect earlier eligibility
Q and short-gap filling	Target chlorophyll is intentional; bounded gaps up to 24 days use both endpoints before annual slicing	Endpoints may lie outside the window; later Q intentionally uses later observations
Feature scaling and ridge fitting	Means, SD, coefficients and intercept use training rows only; validation losses tune alpha	Final fit uses development rows; later exposure inputs are contemporaneous, not advance forecasts
Thermal climatology and event detection	Primary nominal 1982–2011 SST baseline overlaps some target/fold years; no fold refit	Five-day edge expansion can reach January 2012; 1991–2020 sensitivity and full-record detrending use later SST; event persistence can cross window edges
Nitrate climatology	Fixed WOA23 1965–2022 descriptor, not target-year measured nitrate; no fold refit	Product source period overlaps evaluation; individual local contributions are unresolved
Common-support screen	Source-development predictor ranges; no outcome-based screen	Later predictor values determine marginal inclusion, with fixed cases across compared fits

The thermal edge window in the alternative baseline can reach December 1990 and January 2021. Original short-gap eligibility is checked using the full historical curve before target-specific Q reconstruction. The purge audit includes bounded-gap endpoints and composite identities but does not resolve native acquisition dates within nominal composite intervals. Correct fold-local scaling therefore does not make the rest of preprocessing fold-isolated, and shared reference fitting does not by itself prove contamination by later chlorophyll magnitudes.

AI and Programmatic Research Provenance Statement

The originating hypothesis, initial formulation, and initial structure of this work were generated and provided by UCP Technology LLC through its programmatic research process. The source record for the originating research candidate and subsequent development is maintained at: https://github.com/joe-ucp/luigi4

Artificial intelligence was used as a computational component of that process to generate and develop the originating research candidate, including the initial theoretical formulation, research development, manuscript drafting, literature-supported development, and computational verification. Artificial intelligence was not used to provide the independent scientific judgment determining whether the work was correct, useful, novel, or suitable for publication.

The human author independently evaluated, revised, verified, interpreted, and approved the final work.

References

Bengio, Yoshua, and Yves Grandvalet. 2004. "No Unbiased Estimator of the Variance of k-Fold Cross-Validation." *Journal of Machine Learning Research* 5: 1089–1105. https://www.jmlr.org/papers/v5/grandvalet04a.html.

Bergmeir, Christoph, Rob J. Hyndman, and Bonsoo Koo. 2018. "A Note on the Validity of Cross-Validation for Evaluating Autoregressive Time Series Prediction." *Computational Statistics & Data Analysis* 120: 70–83. https://doi.org/10.1016/j.csda.2017.11.003.

Breiman, Leo. 1996. "Heuristics of Instability and Stabilization in Model Selection." *The Annals of Statistics* 24 (6): 2350–83. https://doi.org/10.1214/aos/1032181158.

Cawley, Gavin C., and Nicola L. C. Talbot. 2010. "On over-Fitting in Model Selection and Subsequent Selection Bias in Performance Evaluation." *Journal of Machine Learning Research* 11 (70): 2079–2107. https://www.jmlr.org/papers/v11/cawley10a.html.

European Space Agency. 2023. "Ocean Colour Climate Change Initiative Dataset, Version 6.0." Centre for Environmental Data Analysis. https://doi.org/10.5285/5011d22aae5a4671b0cbc7d05c56c4f0.

Furtado, Jason C., Maria J. Molina, Marybeth C. Arcodia, Weston Anderson, Tom Beucler, John A. Callahan, Laura M. Ciasto, et al. 2026. "Setting the Standard: Recommended Practices for Data Preprocessing in Data-Driven Climate Prediction." *Bulletin of the American Meteorological Society* 107 (6): E1386–1401. https://doi.org/10.1175/BAMS-D-24-0292.1.

Garcia, H. E. et al. 2024. "World Ocean Atlas 2023, Volume 4: Dissolved Inorganic Nutrients (Phosphate, Nitrate, and Silicate)." Atlas NESDIS 92. NOAA. https://doi.org/10.25923/39qw-7j08.

Hastie, Trevor. 2020. "Ridge Regularization: An Essential Concept in Data Science." *Technometrics* 62 (4): 426–33. https://doi.org/10.1080/00401706.2020.1791959.

Hastie, Trevor, Robert Tibshirani, and Jerome Friedman. 2009. *The Elements of Statistical Learning: Data Mining, Inference, and Prediction*. 2nd ed. New York: Springer. https://doi.org/10.1007/978-0-387-84858-7.

Hayashida, Hakase, Richard J. Matear, and Peter G. Strutton. 2020. "Background nutrient concentration determines phytoplankton bloom response to marine heatwaves." *Global Change Biology* 26 (9): 4800–4811. https://doi.org/10.1111/gcb.15255.

Hobday, Alistair J., Lisa V. Alexander, Sarah E. Perkins, Dan A. Smale, Sandra C. Straub, Eric C. J. Oliver, Jessica A. Benthuysen, et al. 2016. "A hierarchical approach to defining marine heatwaves." *Progress in Oceanography* 141: 227–38. https://doi.org/10.1016/j.pocean.2015.12.014.

Huang, B., C. Liu, V. F. Banzon, E. Freeman, G. Graham, W. Hankins, T. M. Smith, and H.-M. Zhang. 2020. "NOAA 0.25-Degree Daily Optimum Interpolation Sea Surface Temperature (OISST), Version 2.1." NOAA National Centers for Environmental Information. https://doi.org/10.25921/RE9P-PT57.

Huang, Boyin, Chunying Liu, Viva Banzon, Eric Freeman, Garrett Graham, Bill Hankins, Tom Smith, and Huai-Min Zhang. 2021. "Improvements of the Daily Optimum Interpolation Sea Surface Temperature (DOISST) Version 2.1." *Journal of Climate* 34 (8): 2923–39. https://doi.org/10.1175/JCLI-D-20-0166.1.

Kapoor, Sayash, and Arvind Narayanan. 2023. "Leakage and the Reproducibility Crisis in Machine-Learning-Based Science." *Patterns* 4 (9): 100804. https://doi.org/10.1016/j.patter.2023.100804.

Moscovich, Amit, and Saharon Rosset. 2022. "On the Cross-Validation Bias Due to Unsupervised Preprocessing." *Journal of the Royal Statistical Society Series B: Statistical Methodology* 84 (4): 1474–1502. https://doi.org/10.1111/rssb.12537.

Noh, Kyung Min, Hyung-Gyu Lim, and Jong-Seong Kug. 2022. "Global chlorophyll responses to marine heatwaves in satellite ocean color." *Environmental Research Letters* 17 (6): 064034. https://doi.org/10.1088/1748-9326/ac70ec.

Oliver, Eric C. J. n.d. "marineHeatWaves: Reference Implementation of the Hobday Marine-Heatwave Definition." https://github.com/ecjoliver/marineHeatWaves.

Roberts, David R., Volker Bahn, Simone Ciuti, Mark S. Boyce, Jane Elith, Gurutzeta Guillera-Arroita, Severin Hauenstein, et al. 2017. "Cross-Validation Strategies for Data with Temporal, Spatial, Hierarchical, or Phylogenetic Structure." *Ecography* 40 (8): 913–29. https://doi.org/10.1111/ecog.02881.

Sathyendranath, Shubha, Robert J. W. Brewin, Carsten Brockmann, Vanda Brotas, Ben Calton, Andrei Chuprin, Paolo Cipollini, et al. 2019. "An Ocean-Colour Time Series for Use in Climate Studies: The Experience of the Ocean-Colour Climate Change Initiative (OC-CCI)." *Sensors* 19 (19): 4285. https://doi.org/10.3390/s19194285.

Simonsohn, Uri, Joseph P. Simmons, and Leif D. Nelson. 2020. "Specification Curve Analysis." *Nature Human Behaviour* 4: 1208–14. https://doi.org/10.1038/s41562-020-0912-z.

Steegen, Sara, Francis Tuerlinckx, Andrew Gelman, and Wolf Vanpaemel. 2016. "Increasing Transparency Through a Multiverse Analysis." *Perspectives on Psychological Science* 11 (5): 702–12. https://doi.org/10.1177/1745691616658637.

Varma, Sudhir, and Richard Simon. 2006. "Bias in Error Estimation When Using Cross-Validation for Model Selection." *BMC Bioinformatics* 7: 91. https://doi.org/10.1186/1471-2105-7-91.

Varoquaux, Gaël. 2018. "Cross-Validation Failure: Small Sample Sizes Lead to Large Error Bars." *NeuroImage* 180: 68–77. https://doi.org/10.1016/j.neuroimage.2017.06.061.

Wyatt, Abigale M., Laure Resplandy, and Adrian Marchetti. 2022. "Ecosystem impacts of marine heat waves in the northeast Pacific." *Biogeosciences* 19 (24): 5689–5705. https://doi.org/10.5194/bg-19-5689-2022.